Ice dynamic and hydrological response to ice-dammed lake drainages at Isunnguata Sermia, West Greenland

Stephen J. Livingstone1, Robert D. Storrar[2], Samuel H. Doyle[1,3], Sian Thorpe[1], Angus Moffatt[1], Andrew J. Sole[1], Thomas R. Chudley[4], Florent Gimbert[5], Joseph A. Graly[6], Kathy Licht[7], Kate Winter[6], Asini Jayarapu[7], Elizabeth A. Bagshaw[8], Guilhem Barruol[5], Kayla Bauer[7], Gianluca Bianchi[9], Sammie Buzzard[6], Caroline C. Clason[4], Lisa Craw[9], Benjamin Davison[1], Laura A. Edwards[10], Bill Gilhooly[7], Trinity Hamilton[11], Chris Hansen[11], Jonathan Hawkins[9], Ryan Ing[12], Moses Jatta[7], Andrew H. Jones[2], Tori Kennedy[7], Siobhan Killingbeck[13], Tifenn Le Bris[5], Rebecca McCerery[6], Alex Messerli[14], Alexandre Michel[5], Felipe Napoleoni[12], Matthew W. Peacey[3], Michael R. Prior-Jones[9], Neil Ross[15], Remy Veness[2], Kayla Woodie[7], Tun Jan Young[16], Adam Hepburn[3], Adam Booth[17]

Corresponding author: s.j.livingstone@sheffield.ac.uk

1School of Geography and Planning, University of Sheffield, Sheffield, United Kingdom
2Geography, Environment and Planning, Sheffield Hallam University, Sheffield, United Kingdom
3Centre for Glaciology, Department of Geography and Earth Sciences, Aberystwyth University, Aberystwyth, United Kingdom
4Department of Geography, Durham University, Durham, United Kingdom
5Univ. Grenoble Alpes, CNRS, INRAE, IRD, Grenoble INP, IGE, 38000 Grenoble, France
6Department of Geography and Environmental Sciences, Northumbria University, Newcastle upon Tyne, United Kingdom
7Earth and Environmental Sciences, Indiana University Indianapolis, Indianapolis, United States
8School of Geographical Sciences, University of Bristol, Bristol, United Kingdom
9School of Earth and Environmental Sciences, Cardiff University, Cardiff, United Kingdom
10School of Biological and Environmental Sciences, Liverpool John Moores University, Liverpool, United Kingdom
11College of Biological Sciences, University of Minnesota, Minneapolis, United States
12School of Geosciences, Edinburgh University, Edinburgh, United Kingdom
13Department of Geography, Faculty of Science and Engineering, Swansea University, United Kingdom
14Asiaq Greenland Survey, Nuuk, Greenland
15School of Geography, Politics and Sociology, Newcastle University, Newcastle upon Tyne, United Kingdom
16School of Geography & Sustainable Development, University of St Andrews, St Andrews, United Kingdom
17School of Earth and Environment, University of Leeds, Leeds, United Kingdom

ABSTRACT

Ice-marginal lakes are increasingly common around Greenland and are important for modulating glacier runoff and dynamics. This study investigates the evolution of a ~3 km^2 and up to ~100 m deep ice-dammed lake at Isunnguata Sermia, West Greenland. Satellite observations between 1987 and 2024, and field observations of a 2023 drainage using passive seismics, GNSS and time-lapse imagery reveal that the lake drains subglacially and has undergone 12 fill-drain cycles since 1987, a drainage periodicity of 1-3 years. Peak lake volume has decreased since 2010, associated with glacier thinning. Lake drainage can perturb the wider subglacial hydrology system, including triggering the release of stored subglacial water along the flood path in 2019. During the extreme melt year of 2012, the lake drained but did not refill, suggesting that subglacial leakage under

the ice dam was sustained by record runoff. Transient ice flow acceleration was observed during the late season drainage in 2023 when the subglacial hydrological system was less efficient and therefore more easily overwhelmed. Our results indicate that ice-dammed lake fill-drain cycles, and the downstream impact on subglacial hydrology and ice dynamics, are modulated by ice dam thickness, melt supply and the antecedent subglacial hydraulic capacity.

INTRODUCTION

Ice-marginal lakes form as water becomes dammed behind ice or moraines, or trapped in overdeepened basins. Over 3300 ice-marginal lakes exist around the fringe of the Greenland Ice Sheet (GrIS) (How and others, 2021), constituting ~10% of the ice margin (Carrivick and others, 2022). The number of ice-marginal lakes in Greenland has increased over the last three decades, likely in response to enhanced meltwater runoff and glacier recession (Carrivick and Quincey, 2014; How and others, 2021). This is significant as lakes trap sediment and nutrients, delay the transfer of water to the ocean (Carrivick and Tweed, 2013), and can accelerate glacier recession and mass loss (Kirkbride, 1993; King and others, 2019; Sutherland and others, 2020; Mallalieu and others, 2021).

Ice-dammed lakes can drain catastrophically, producing high-magnitude floods, known as glacial lake outburst floods (GLOFs) or jökulhlaups (e.g., Thórarinsson, 1939; Liestøl, 1956). GLOFs have been well studied around the world (see Lützow and others, 2023 for a global database) due to the hazard they pose to communities (e.g., Post and Mayo, 1971; Haeberli, 1983; Carrivick and Tweed, 2016), their downstream ecological and geomorphological impact (e.g. Russell and others, 2006, 2011; Tomczyk and others, 2020) and their potential to modify ice dynamics (e.g., Einarsson and others, 2016). Ice-dammed lakes slowly (months to years) accumulate meltwater and rainfall before rapidly (days to weeks) draining due to unstable failure of the ice dam. Potential dam failure mechanisms include dam flotation (Thórarinsson, 1939; Glen, 1954), syphoning by the subglacial drainage system (Whalley, 1971), breaches between the ice dam and bedrock (Haeberli, 1983; Walder and Costa, 1996) and Darcian flow through basal sediments (Fowler and Ng, 1996).

During the rising flood stage of a subglacial GLOF, hydrographs are typically characterised by exponentially- (‘slow’) or linearly- (‘fast’) rising discharge. Slow drainage is thought to be controlled by the opening of a subglacial channel due to a positive feedback between the rate of frictional melting of its ice walls and frictional heat generated by the turbulence of the water flowing through it (Nye, 1976). Fast lake drainage is caused by the initial hydraulic uplift of the ice by a sheet flood rather than drainage through a discrete conduit(s) (Björnsson, 1992; Flowers and others, 2004; Einarsson and others, 2017). The hydraulic gradient driving water flow is controlled by the lake level and therefore decreases as the lake drains, eventually resulting in rapid termination as channel closure by ice deformation exceeds melt opening (Nye, 1976). This resealing of the ice dam allows water to begin accumulating again, consequently leading to cyclic fill-drain behaviour. Temporal trends suggest that over time the magnitude of GLOFs from ice-dammed lakes globally have decreased (Rick and others, 2023; Veh and others, 2023), consistent with glacier mass loss reducing the thickness of the ice dam and thus the maximum lake level (Thórarinsson, 1939; Matthews and Clague, 1993; Evans and Clague, 1994).

GLOFs are relatively under-studied in Greenland compared to other glaciated regions of the world, such as Iceland and the Himalayas (Lützow and others, 2023) and there are limited multi-decadal records, which are important for determining controls on flood timing and size, as well as drainage mechanisms (Ng and Liu, 2009). However, they are likely to be common events, with a recent study identifying 326 lakes in Greenland experiencing a total of 541 GLOFs between 2008 and 2022 (Dømgaard and others, 2024). This includes rapid (days) drainage of large (>1 km^3) volumes of water (e.g., Kjeldsen and others, 2017; Grinsted and others, 2017; Carrivick and Tweed, 2019). In this paper, we investigate the evolution of a ~3 km^2 ice-dammed lake adjacent to the northern margin of Isunnguata Sermia, West Greenland (Fig. 1). This lake was included in the GLOF inventory of Dømgaard and others, (2024), with drainages detected in satellite imagery in 2010, 2020 and 2022, but based on only 18 observations spanning 2008-2022. We build on this work, using optical imagery and time-stamped Digital Surface Models (DSMs) to comprehensively reconstruct lake-level evolution since 1987. This analysis allows us to determine controls on flood frequency and magnitude, and its downstream impacts. Field measurements are used to analyse the hydraulic and glaciodynamic processes of the most recent GLOF in 2023.

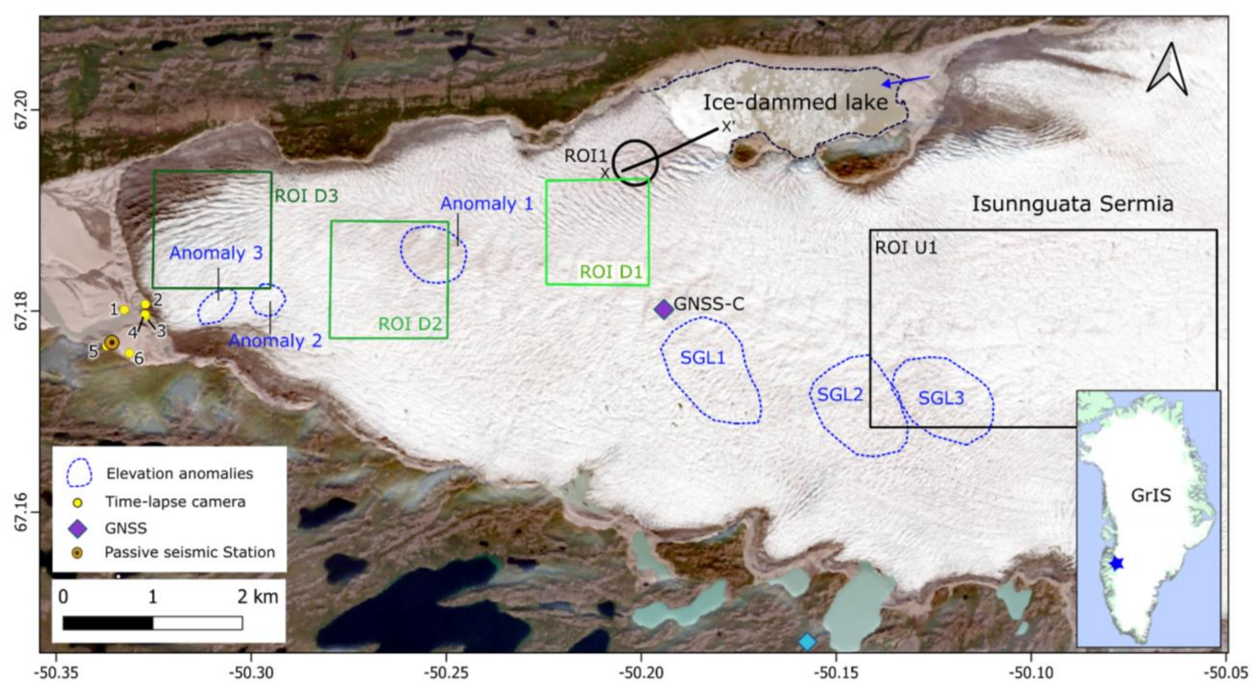

Figure 1. Location of Isunnguata Sermia, West Greenland (blue star in inset map) and ice-dammed lake at the northern margin of the ice tongue. Region of Interest (ROI) 1 (black circle) is used to calculate median ice thickness change of the glacier downstream of the ice-dammed lake from ArcticDEM strips. Cross profile x-x' is used to calculate ice-surface elevation profiles for Fig. 4a. ROIs D1-3 (downstream of the lake) and U1 (upstream of the lake) are used to calculate velocities from feature tracking (see Methods). Blue dashed polygons represent ice-surface elevation anomalies. SGL1-3 are anomalies (expected to represent subglacial lakes) previously reported in Livingstone et al., (2019). Anomalies 1-3 are reported herein. Scientific instruments were installed in summer 2023 and captured the GLOF that occurred in the autumn of the same year. Time-lapse cameras are labelled 1-6. Background is Sentinel-2 optical imagery (2024-08-13). Note river inflow (blue arrow) at the eastern end of the lake, originating from under Isunnguata Sermia.

DATA AND METHODS

Ice-dammed lake evolution - Remote Sensing (1987-2024)

To evaluate the long-term evolution of the ice-dammed lake, shorelines were manually digitized from 313 optical satellite images and time-stamped ArcticDEM DSM strips between 1987 and June 2024. USGS/NASA Landsat 5-8 (30 m resolution), ASTER (15 m resolution) and Sentinel-2 (10 m resolution) imagery was digitized using the Google Earth Engine Digitisation Tool (GEEDiT) v. 2.03 (Lea, 2018). This was supplemented by images from Planet Labs that were acquired using the 3 m resolution PlanetScope instrument. Time-stamped ArcticDEM DSM strips at 2 m resolution (Porter et al., 2023) were extracted and co-registered using the *pDEMtools* python package (Chudley and Howat, 2024). Co-registration was performed against the ArcticDEM mosaic following Nuth and Kääb (2011), with stable ground identified using the BedMachine v5 (Morlighem and others, 2022) land mask. Shorelines for both ArcticDEM strips and Planet imagery were manually digitized in QGIS v3.34. Shoreline digitization involved mapping the boundary between water and land for regions where the edge of the lake could be clearly discriminated. Images obscured by clouds or where the presence of icebergs made it difficult to identify the shoreline were excluded from the dataset. Shoreline elevations were extracted from the bathymetry determined using the co-registered 2019-08-11 ArcticDEM DSM strip when the lake was fully drained.

Median elevations were calculated for each time-stamped lake-shoreline. The uncertainty in shoreline-derived lake levels was calculated from the standard deviation (1σ) of elevation values, with the lower image resolutions typically resulting in greater uncertainty (mean uncertainty: ± 9.4 m for Landsat; ± 5.4 Planet; ± 4.7 for ArcticDEM). Lake shoreline elevations were converted to volume using the *Surface Water Storage* plugin in QGIS, based on the 2019-08-11 ArcticDEM DSM strip, producing a scaling relationship between lake shoreline elevation and lake volume (Fig. S1). Volume uncertainties were calculated by applying the elevation-volume scaling relationship to the standard deviation of elevation values. We do not account for errors associated with variations in glacier front position and stranded icebergs in the ArcticDEM DSM strip. Freeboard was calculated by manual picking of the ice surface elevation at the front of the calving face, along a transect orientated normal to the ice margin and aligned with the centre of the lake. The minimum value along this transect was used to identify the lake surface height, which was subtracted from the ice surface height.

The downstream impacts and footprint of each GLOF were investigated using optical satellite imagery in GEEDiT. This included identifying large calving events linked to, or preceding, the GLOF, coincident drainages of smaller downstream ice-dammed lakes, and flood limits of the proglacial braided river system.

To investigate the coupling between lake fill-drain cycles and ice-surface elevation change, median and median absolute difference (MAD) ice surface elevation was calculated. This was done within a 500 m diameter region of interest ~500 m upstream of the main lake calving front for 51 co-registered ArcticDEM DSM strips between 2009 and 2023 (Fig. 1, ROI1). Ice surface elevation profiles across the main calving front (Cross-profile x-x’ in Fig. 1) were used to extract changes in ice surface, lake height and freeboard of the ice-front from the ArcticDEM.

Ice-surface elevation anomalies (Fig. 1, anomalies 1-3) occurred at the same time as some lake drainage events. Following Livingstone and others (2019), relative elevation changes for each anomaly were calculated by subtracting the mean ice-surface elevation of the anomaly from the mean elevation of a 500 m buffer around it. This approach allowed the dynamic effect to be isolated from longer term thinning signals, and to remove the influence of any vertical and horizontal offsets between DSMs.

Ice surface motion (2016-2024)

Ice-surface velocity was estimated from feature and speckle tracking of Sentinel-1a (2014/4 - present) and Sentinel-1b (2016/4 - 2021/12) Interferometric Wide swath mode Single-Look Complex Synthetic Aperture Radar (SAR) amplitude images. We used approximately 2000 Sentinel-1a/b 12-day repeat-pass image pairs between January 2016 and May 2025. Prior to tracking, Sentinel image pairs were focused and co-located using the Generic Mapping Toolbox for SAR imagery (GMTSAR; Sandwell et al., 2011a, 2011b). Each image was split into many overlapping 'image patches', with tracking of each image patch undertaken in MATLAB, within a version of PIVsuite (Thielicke and Stamhuis, 2014; https://uk.mathworks.com/matlabcentral/fileexchange/45028-pivsuite) adapted for ice flow (Tuckett and others, 2019; Davison and others, 2020). Ice velocity data from all coincident image pairs were filtered for anomalous data, mosaicked, co-located and stacked. The stacked data were smoothed using a 3x3 pixel moving median kernel and resampled to 200 m. Additional filtering of the stacked data based on temporal variations in velocity magnitude and flow direction removed remaining spurious estimates.

Time series of ice motion were created by taking the median value from within regions of interest (Figure 1); one upstream of the lake drainage (U1) and three downstream (D1-3). All 12-day velocity estimates from within each ROI were smoothed using a second degree 24-day Savitsky-Golay filter. Analysis of apparent motion over non-moving bedrock areas indicates average uncertainties of 20 - 50 m/yr.

Field measurements of 2023 lake drainage

During late September and early October 2023 a range of sensors placed on and in-front of Isunnguata Sermia recorded a GLOF associated with subglacial drainage of the ice-dammed lake.

Time-lapse camera imagery and proglacial river stage

Six SLTL-6210MC Plus 12 Megapixel Scouting time-lapse cameras were installed near the margin of Isunnguata Sermia (Fig. 1) to monitor subglacial upwelling and proglacial accreted ice between September 2022 and April 2024. Each camera took 4 repeat photos per day from 11:00 – 14:00; each photo is time- and temperature-stamped.

Time lapse imagery from camera 3 (Fig.1) was used to find the relative stage of a section of the braided proglacial river during the ice-dammed lake drainage. The Segment Anything Model (SAM; Kirrillov and others, 2023) was used to create a mask of the river for each time lapse image. From this, a mean average height of the wetted shoreline was calculated in the region where the shoreline is against the quasi-vertical bank, thus providing the most representative estimate of river surface height (Fig. S2). The shoreline position was then converted from pixels to metres with respect to a reference measurement taken when the camera was deployed. Stage is displayed relative to the lowest stage during this period.

Ice surface motion

Time series of horizontal and vertical ice surface motion were determined from dual frequency (L1 + L2) Global Navigation Satellite System (GNSS) data recorded by a Leica GS10 receiver at 0.1 Hz. GNSS station C was located at 67.186N, -50.203W, 2.0 km south of the ice-dammed lake and 5.8 km east of the glacier terminus (Fig. 1). The GNSS antenna was mounted on a 6-m-long aluminium pole drilled 5 m into the ice surface. Rapid re-freezing of the hole secured the antenna pole within the ice. Data were post-processed kinematically (King, 2004) relative to a bedrock-mounted reference station using the differential carrier-phase positioning software Track v1.53 (Chen, 1998). The baseline length was 4.0 km and precise ephemerides from the International GNSS Service were used (Dow and others, 2009). Positioning uncertainties were estimated at ~0.01 m in the horizontal and ~0.02 m in the vertical by calculating the standard deviation of the residuals from linear regression applied to the position time series during a month-long period of steady ice motion in November 2023. Small (< 5 min) gaps in the position record were linearly interpolated before a second-order 6 h low-pass Butterworth filter was applied. The position record was then resampled to 10 minute medians and differentiated to calculate velocity, which was further filtered using a 6 h moving average. Daily mean velocities were calculated from the filtered 10-min interval velocity record. To prevent phase shifts, phase preserving filters, differentiation, and resampling methods were used throughout.

Passive seismic

A Digos DATA-CUBE^3 Type 2 data logger with a 4.5 Hz 3-component geophone sampling at 100 Hz was installed adjacent to the proglacial river (Fig. 1) to measure seismic tremor generated by river discharge. This approach follows previous studies which found a correlation between seismic noise in the 2 – 10 Hz frequency range and water discharge, attributed to turbulent flow in the river channel (Schmandt and others, 2013; Díaz and others, 2014; Gimbert and others, 2014). Seismic power was calculated using Welch's averaging method (Welch, 1967) applied to the vertical component of ground motion, on 3 s time windows with 50% overlap. Power was averaged over 60 s time windows.

Surface melt estimates

To estimate daily surface runoff (melt plus rain)n at GNSS-C we used COSIPY - a COupled Snowpack and Ice surface energy and mass-balance model in PYthon (see Sauter and others, 2020). We forced this model with data from the PROMICE KAN_L automatic weather station situated at ~630 m a.s.l. approximately 14 km SE of the ice-dammed lake (Fausto and others, 2021) and precipitation data from the nearest ERA5 Land reanalysis model grid cell (Muñoz Sabater and others, 2019). Air temperatures were interpolated to the elevation of GNSS-C using a constant lapse rate of -5.3 °C km^{-1} and air pressure was interpolated using the barometric equation.

RESULTS

Ice-dammed lake evolution (1987-2024)

Shoreline mapping of the ice-dammed lake revealed 12 fill-drain cycles between 1987 and 2024 (Fig. 2). Prior to the launch of the Landsat 7 satellite in 1999, data are sparser with at least one GLOF likely missed between 1987, when the lake was relatively full (0.164 ± 0.044 km^3), and 1993 when the lake was filling from a lower level (0.077 ± 0.035 km^3). Lake evolution is characterised by slow filling over 1-3 years (mean: 2.8 years), with satellite imagery indicating recharge from water emanating from under ice flowing into the eastern side of the lake (Fig. 1). Filling is followed by rapid subglacial drainage beneath the southwest ice-contact boundary of the lake. There is a clear seasonal pattern of filling; lake levels typically rise by 40-50 m during the summer melt season (June-August), with slower filling towards the start and end, while the winter (October-March) is characterised by no significant (i.e. within error) or slow increases in water level (Fig. 2).

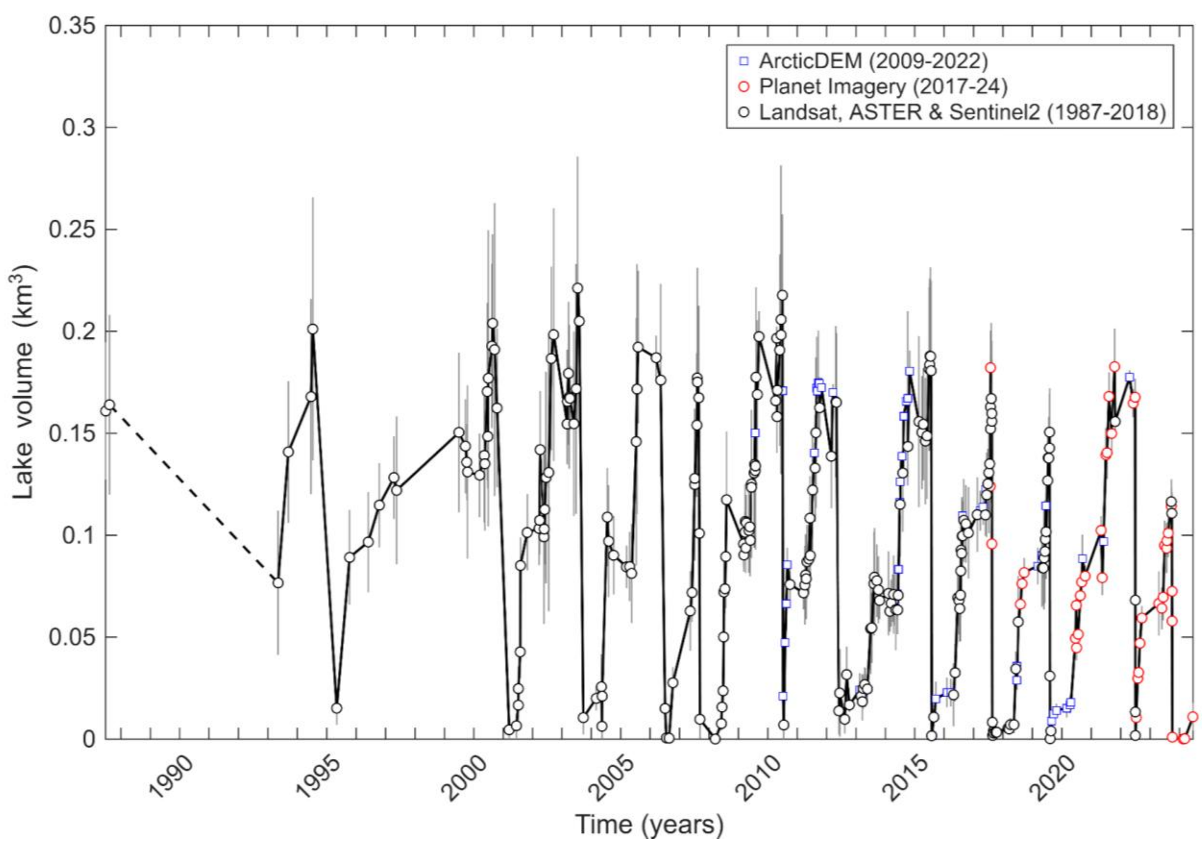

Figure 2. Ice-dammed lake volume evolution (1987-2024) based on shorelines mapped using optical imagery and the time-stamped ArcticDEM strips, and application of an elevation-volume scaling relation (see methods and Figure S1). Note that 1987 to 1993 is poorly constrained (black dashed line). See Methods section for details of error bars.

Lake drainages occur throughout the melt season, ranging from May-June (e.g., 2012) through to late September / early-October (e.g. 2023), but with the majority (at least 6) occurring between July and August when melt tends to be greatest. The lake volume at which drainage occurs varies, but with a statistically significant negative relationship (Pearson $r = -0.71$, $p<0.05$) through time (Fig. 3a, Fig. S3). Up to 2010, lake volumes reached >0.176 km^3 (>365 m a.s.l.) before drainage occurred, with a peak lake volume of 0.218 ± 0.04 km^3 (218 million cubic metres) recorded during the 2010 drainage. Since 2010, 50% of the drainages have occurred at lake volumes <0.176 km^3, with the 2019 and 2023 levels peaking at just 0.151 ± 0.019 km^3 and 0.111 ± 0.01 km^3 respectively. This ~0.05 km^3 reduction in volume and 20 m drop in maximum lake level since 2010 corresponds with a ~10 m reduction in median ice-surface elevation within ROI1, dropping from ~413 m a.s.l. in 2010 to ~403 ± 4.9 m a.s.l. in 2023 (Figs. 3a and 4a). Within ~200 m of the calving-front, Isunnguata Sermia responds to changes in lake level (Fig. 4a), lifting up to 37 m as the lake becomes full and the ice likely begins to float (Fig. 4b). The freeboard height during periods when the lake is full and the ice-front is floating is 12-16 m, which corresponds to a maximum ice thickness of 145-193 m assuming hydrostatic equilibrium, an ice density of 917 kg m^3 and water density of 1000 kg m^3. The lake basin is completely or nearly emptied during GLOFs, with the lake level dropping around 100 m and the freeboard height increasing (Fig. 4b). The denser temporal record of satellite observations from 2009 onwards has enabled 6 GLOF events to be constrained to <10 days, with the 2022 event occurring in just 4 days or less (Table 1), with a minimum mean discharge of 480 $m^3 s^{-1}$.

The downstream ice velocity response to drainage of the ice dammed lake is variable (Fig. 5). Of the four drainage events within the window of the Sentinel-1 ice velocity data (2016-2025), there was no discernable impact on ice flow during the 2017 and 2019 events, but a relative increase in ice flow at downstream sites during the 2022 and 2023 events. The 2022 drainage event was associated with a 20-60% speed-up at downstream ROIs compared to the upstream ROI, whilst the 2023 event coincided with a 50-110% relative acceleration, which was the largest GLOF and non-GOLF-related velocity anomaly between 2016-2025.

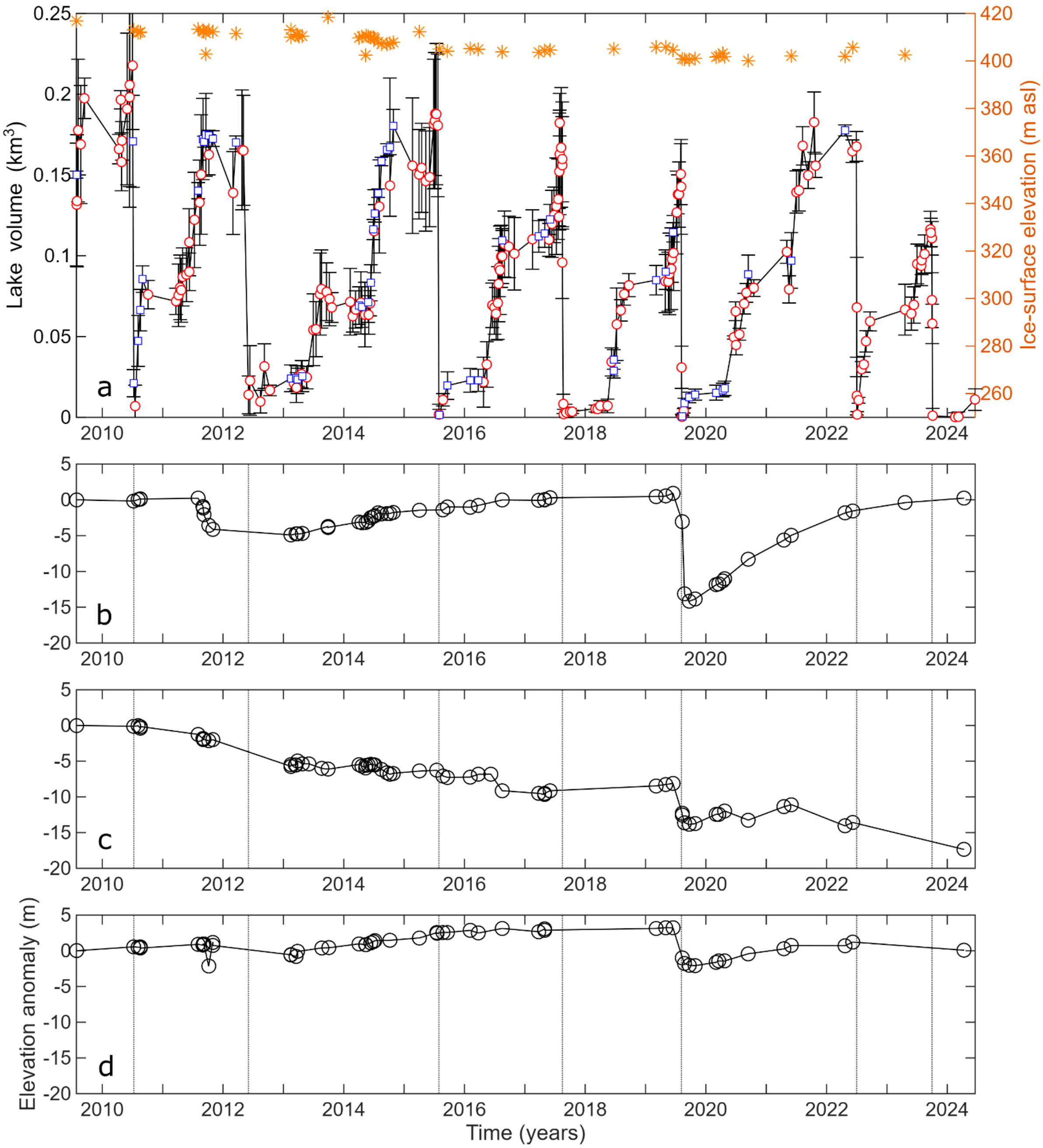

Figure 3. (a) Time series of ice-dammed lake volume (black line; symbols are the same as Figure 2) and median ice-surface elevation (orange stars, ROI1 in Fig 1) from 2009 to 2024. See Methods Section for details of error bars. (b-d) Time series of mean relative ice surface elevation from 2009 to 2024 for three ice-surface elevation anomalies on Isunnguata Sermia (see Fig. 1) (b-d). (b) Anomaly 1; (c) Anomaly 2; (d) Anomaly 3. Vertical dotted lines mark drainage events of the ice-dammed lake visible in (a).

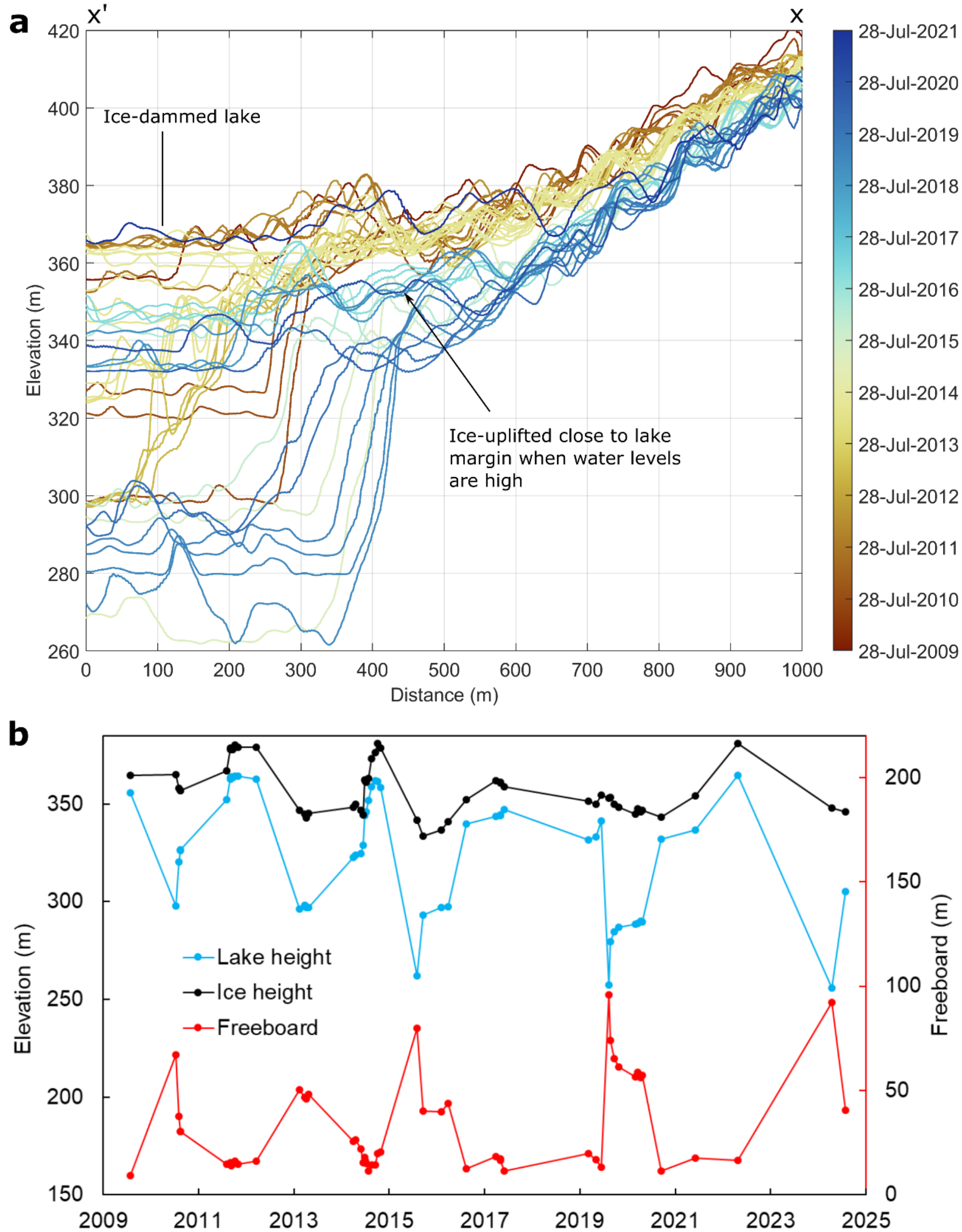

Figure 4. (a) Cross-profile showing ice-lake interactions at the calving front from 2009-2022 based on ArcticDEM DSM strips along profile x-x' in Fig. 1. Note the overall pattern of declining elevation (ice thinning) over the 13-year period, with ~10 m thinning furthest upglacier and nearly 40 m thinning within 100 m of the lake. Within 200 m of the lake, the ice surface is uplifted when the lake is filled. (b) Lake height, ice-height and freeboard (difference between the two) calculated from the ArcticDEM DSM (2009-2024). Note that not all drainage events are captured by the ArcticDEM alone.

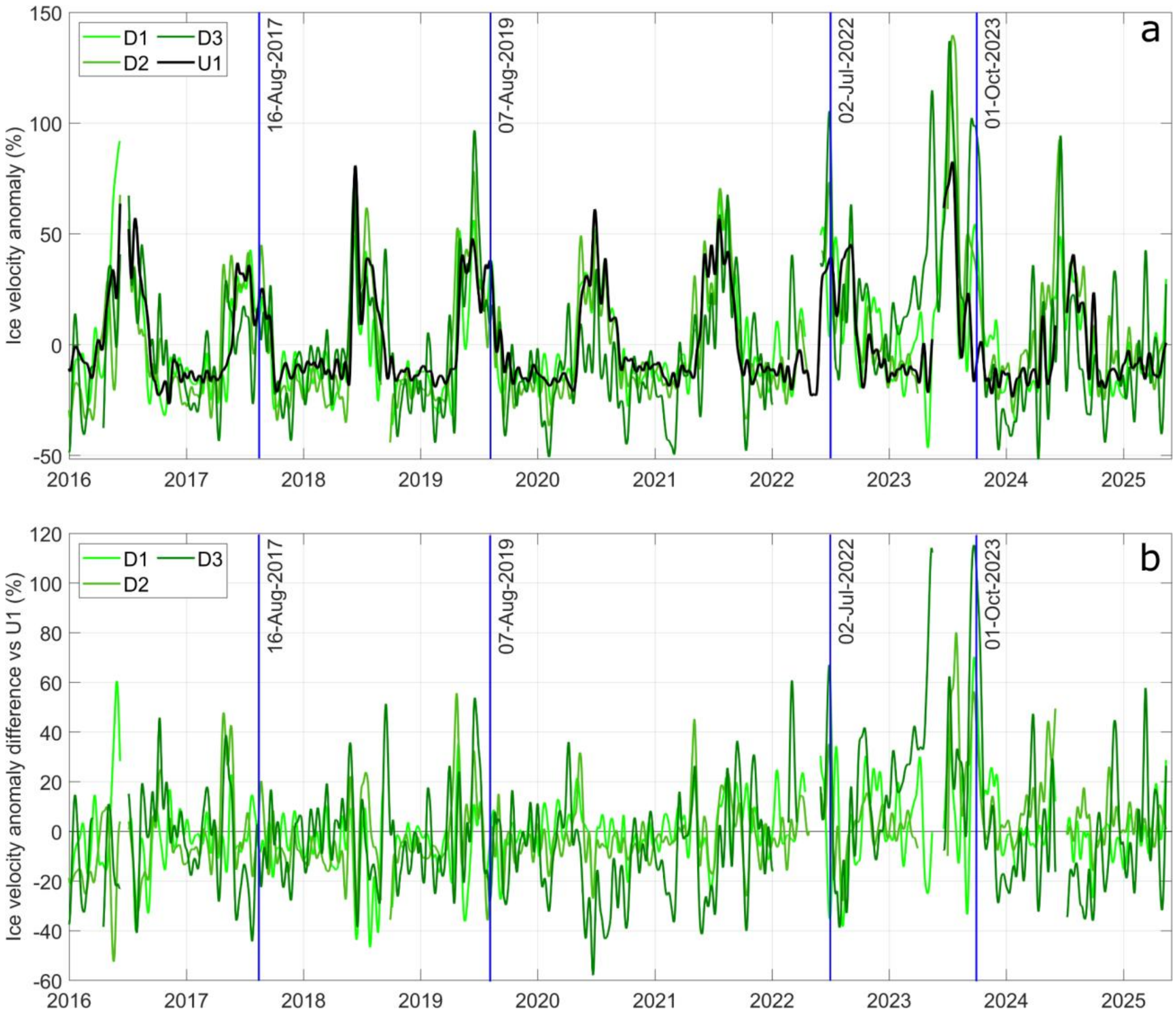

Figure 5. (a) Ice velocity temporal anomaly compared to the whole time period mean for three ROIs (see Figure 1 for locations). U1 is upglacier and D1-3 are downglacier from the ice dammed lake. Vertical blue lines and labels mark the first satellite record of each ice-dammed lake drainage (see Table 1). Subplot (b) shows the difference between the ice-velocity anomalies for D1-3 and U1. Note that both the 2022 and 2023 lake drainage events coincide with a large positive anomaly indicating a relative speed up of the downstream ROIs. The raw time series for each ROI are shown in Figure S4.

Table 1. Dates of ice-dammed lake drainage based on satellite imagery (yyyy-mm-dd). This includes the dates immediately pre-, during and post-drainage, and associated lake volumes and water levels. The drainage duration is the number of days between the pre- and post-drainage imagery. Drainage durations were only noted where they can be reasonably constrained by satellite imagery and the ArcticDEM. The satellite imagery used to identify the lake shorelines is noted in brackets. L = Landsat and S = Sentinel.

Drainage dates and source	**Lake volume (km^3) and *[lake level (m a.s.l.)]***

Pre-drainage	**Drainage & post-drainage**	**Pre-drainage**	**Post-drainage**	**Drainage duration**
1994-07-12 (L5)	1995-05-05 (L5)	0.201 ± 0.065 *[373 ± 9.3]*	0.015 ± 0.008 *[291 ± 4.7]*	
2000-09-17 (L7)	2001-03-17 (L7)	0.191 ± 0.072 *[370 ± 10.6]*	0.005 ± 0.013 *[275 ± 12.9]*	
2003-08-05 (ASTER)	2003-09-24 (L7)	0.205 ± 0.014 *[374 ± 2.0]*	0.011 ± 0.008 *[285 ± 5.8]*	
2006-05-11 (L7)	2006-07-05 (ASTER) 2006-07-21 (ASTER)	0.176 ± 0.047 *[365 ± 7.1]*	0.015 ± 0.005 *[291 ± 2.7]* 0.001 ± 0.005 *[262 ± 10.3]*	
2007-08-27 (L7)	2007-09-12 (L7)	0.167 ± 0.045 *[363 ± 6.9]*	0.010 ± 0.010 *[284 ± 7.1]*	
2010-07-02 (L7)	2010-07-10 (ArcticDEM) 2010-07-18 (L7)	0.218 ± 0.040 *[377 ± 5.6]*	0.021 ± 0.008 *[297 ± 4.1]* 0.007 ± 0.013 *[280 ± 11.0]*	8 days
2012-05-04 (L7)	2012-06-03 (L7)	0.165 ± 0.034 *[362 ± 5.2]*	0.014 ± 0.012 *[289 ± 7.1]*	
2015-07-24 (L8)	2015-07-31 (L8)	0.181 ± 0.044 *[366 ± 6.5]*	0.002 ± 0.007 *[266 ± 10.3]*	7 days
2017-08-15 (S2)	2017-08-16 (Planet) 2017-08-21 (S2) 2017-08-24 (S2)	0.160 ± 0.026 *[360 ± 4.1]*	0.096 ± 0.022 *[338 ± 4.3]* 0.008 ± 0.006 *[282 ± 4.7]* 0.002 ± 0.003 *[267 ± 5.6]*	9 days
2019-08-02 (S2)	2019-08-07 (S2) 2019-08-09 (S2) 2019-08-11 (ArcticDEM)	0.151 ± 0.019 *[355 ± 4.7]*	0.031 ± 0.013 *[306 ± 5]* 0.0003 ± 0.002 *[259 ± 4.8]* 0.001 ± 0.001 *[261 ± 1.6]*	5 days
2022-06-30 (S2)	2022-07-02 (S2) 2022-07-03 (L9) 2022-07-04 (S2)	0.168 ± 0.009 *[362 ± 1.4]*	0.068 ± 0.031 *[327 ± 7.0]* 0.013 ± 0.012 *[289 ± 7.3]* 0.002 ± 0.002 *[267 ± 3.2]*	4 days
2023-09-30 (S2)	2023-10-01 (Planet) 2023-10-02 (Planet) 2023-10-05 (Planet)	0.111 ± 0.010 *[344 ± 1.9]*	0.072 ± 0.017 *[329 ± 3.7]* 0.058 ± 0.012 *[322 ± 3]* 0.001 ± 0.005 *[264 ± 8.9]*	5 days

2019 GLOF - Cascade of downstream subglacial events

The 2019 GLOF drained 0.12 km^3 over ~5 days, with the lake level dropping 98 m between the 4th and 9th August (Table 1, Fig. 6). This gives a mean discharge of 278 m^3 s^{-1}, which is likely to underestimate peak discharge. The foreland showed limited evidence of a change in river stage during and following the ice-dammed lake drainage (Fig. 6). However, the GLOF generated a cascade of downstream subglacial events detected from repeat ArcticDEM DSM data and optical imagery. Downstream of the lake three quasi-circular regions of the ice surface subsided during the same period

(Anomalies 1-3 in Figure 7a). Time series of relative elevation change for each anomaly (Fig. 3b-d) suggest similar behaviours, with subsidence starting between 16th June and 11th August, which was largely complete by 25th August and at its lowest level on 22nd September. Given the subsidence persisted after 11th August when the ice-dammed lake was fully drained, we suggest these events were most likely triggered by the GLOF, although we lack the temporal resolution to confirm this.

Anomaly 1 is located 2.6 km downstream of the ice-dammed lake at the western end of a large overdeepened trough where the ice is ~230 m thick (Fig. 7b). A 0.36 km^2 surface depression with a mean drop of 15 m and maximum drop of 38 m formed between 16th June and 22nd September 2019 (Fig. 3b). Anomalies 2 and 3 are both located within 1.5 km of the glacier terminus, close to the main meltwater outlet and above relatively thin ice (120-130 m). They formed 0.11 and 0.10 km^2 depressions respectively, with mean surface lowering of 5.2 and 5.7 m and maximum surface lowering of 14 and 16 m across the same period (Fig. 3c-d). Across the full time-series, Anomalies 1 and 3 are characterised by periods of slow uplift followed by rapid subsidence, similar to the three ice-surface elevation patterns previously detected further to the east (SGL 1-3 in Figure 1). These were previously interpreted as recording subglacial lake filling and drainage (Livingstone et al., 2019). Anomaly 1 previously underwent a 4.3 m mean elevation drop between 3rd August and 31st October 2011, with crescentic crevasses apparent on the ice surface in 2012. Anomaly 3 also subsided between 31st October 2011 and 14th February 2013, and might therefore be associated with the 2012 GLOF, although the drainage event is poorly constrained. Anomaly 2 is characterised by a long-term trend of subsidence relative to the surrounding ice surface. There is a more subtle (few metres) pattern of subsidence, evident between 6th June 2019 and 22nd September 2019 (Fig. 7a). This subsidence, which follows the W-E axis of the basal overdeepening across Anomaly 1 (Fig. 7b) southwards towards Anomaly 2 and then west to the outflow at the terminus, suggests the wider pattern of subglacial drainage is associated with the anomalies and represents a potential drainage flowpath during GLOFs (arrows on Figure 7a).

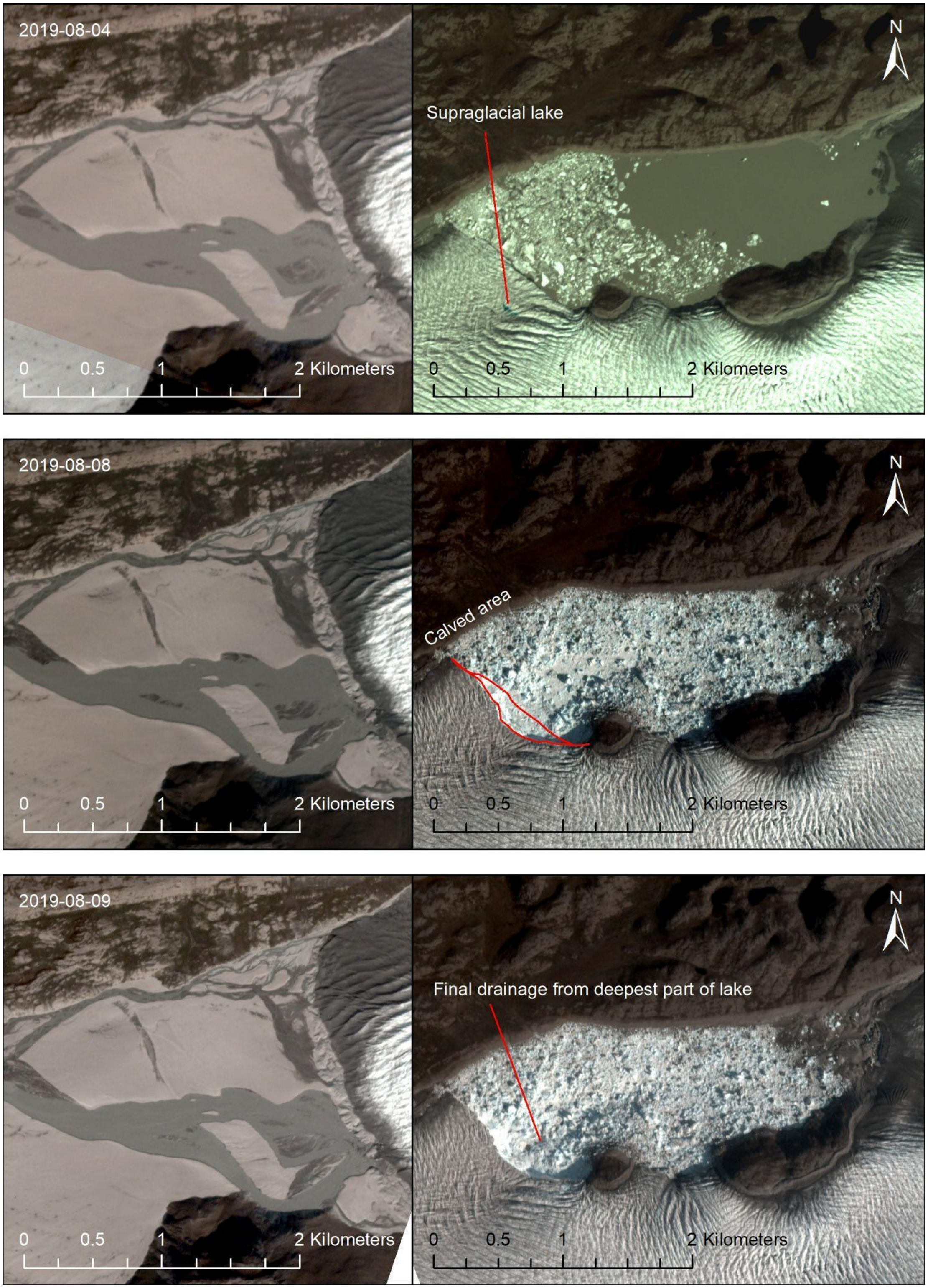

Figure 6. Cloud-free true colour optical satellite imagery (PlanetScope) of the terminus (left column: note the absence of significant changes to the proglacial river and floodplain) and ice-dammed lake (right column) before (4th August), towards the end of (8th August) and after (9th August) the 2019 drainage event. Images © 2019 Planet Labs PBC.

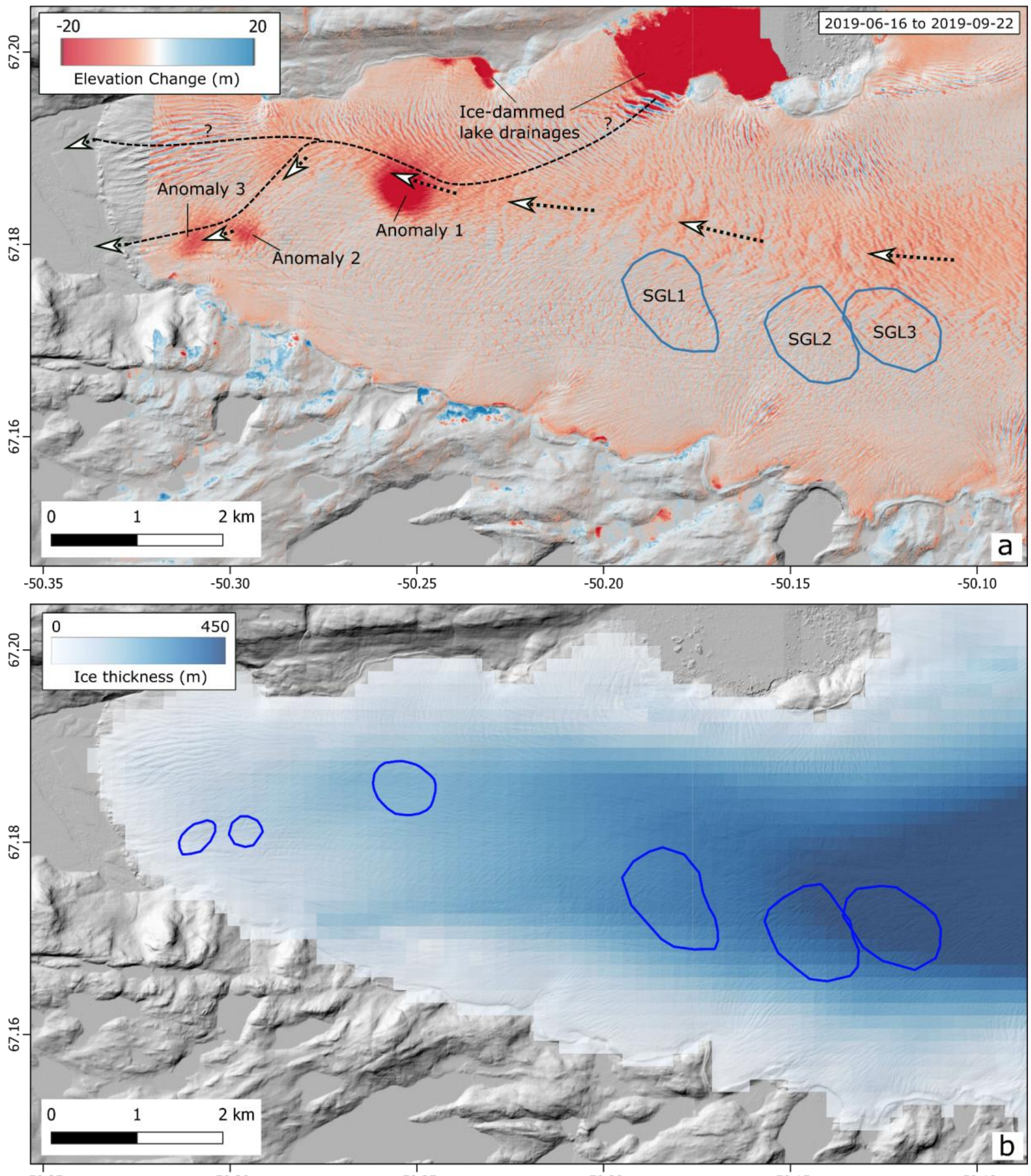

Figure 7. (a) Anomaly plot of ice-surface elevation change from 2019-06-16 to 2019-09-22 from differencing ArcticDEM DSMs. Dashed arrows represent the interpreted subglacial drainage pathways based on the pattern of ice-surface subsidence. The long-dashed line emanating from the ice-dammed lake represents the inferred lake drainage pathway based on both the pattern of subsidence and changes in proglacial river stage. Note during the period the ice-dammed lake drained, three areas of the ice surface subsided (anomalies 1-3). (b) Ice thickness based on the Bedmachine v5 DEM (Morlighem et al., 2017).

2023 GLOF - remote sensing and field observations

Remote sensing observations

Satellite imagery of the ice-dammed lake shows that it drained 0.11 km^3 over 5 days between 30th September and 5th October 2023, with the lake level dropping 80 m (Table 1, Fig. 8). This drainage corresponds to a mean discharge of 255 m^3 s^{-1} across the 5 days, with a mean of ~471 m^3 s^{-1} across a 23 hour period between 30th September and 1st October. During drainage between the 1st and 2nd October, there was a 89,669 m^2 calving event from the glacier terminus into the ice-dammed lake. Between the 1st and 2nd October water ponded on the ice surface towards the northern terminus (Fig. 8). The lack of ponding off-ice, the origin at crevasses and the drop in elevation towards the margin, suggest this water rose to the ice surface from the bed through the crevasses during the GLOF.

Increased proglacial river flow is observed in both satellite and time-lapse imagery from 24th September, despite low rainfall and melt, suggesting that lake drainage could have begun earlier (Figs. 8-10). This includes an increase in water levels from 25th September recorded by time-lapse cameras (e.g., Fig. 9), increased activity of the northern proglacial river system and an increase in stage in the southern proglacial river system between the 24th and 30th September (Fig. 8).

Time-lapse photography at 67.181N -50.334W (camera 4 in Fig. 1) began on 21st September 2023. The camera pointed westward, across a stream between the Isunnguata Sermia terminus and a subglacial upwelling (Fig. 9). Here, turbulent subglacial waters emerged into an area of ponded water surrounded by accreted ice, which overlay the outwash plain. The water level recorded by the time-lapse camera slowly fell from 11:00 (local Western Greenland Time) on 21st September until 13:00 on 25th September. One hour later, the water began rising. By 11:00 on 26th September, the water had risen and at 11:00 on 27th September, another increase in water level was visible. During this period, no turbulent upwelling was evident. At 11:00 on 28th September, water overflowed its basin and the point of emerging water was apparent in the same position as 21st September. By 29th September, the emerging waters began erupting higher than the surrounding accreted ice. Additionally, a mound of dislodged accreted ice or frozen outwash appeared in the pond overnight. These mounds disappeared on 30th September and were replaced by other mounds, including a prominent one in the foreground of the image. The eruption height reached a maximum on 1st October and continued through 2nd October. By 11:00 on 3rd October, the water level fell while vigorous eruptions continued. This is consistent with satellite imagery indicating that between the 3rd and 5th October the northern proglacial river had returned to its previous state and the southern river had decreased in stage. In the 11:00

photograph on 5th October, the eruption had ceased and ponded water drained, leaving a landscape of accreted ice.

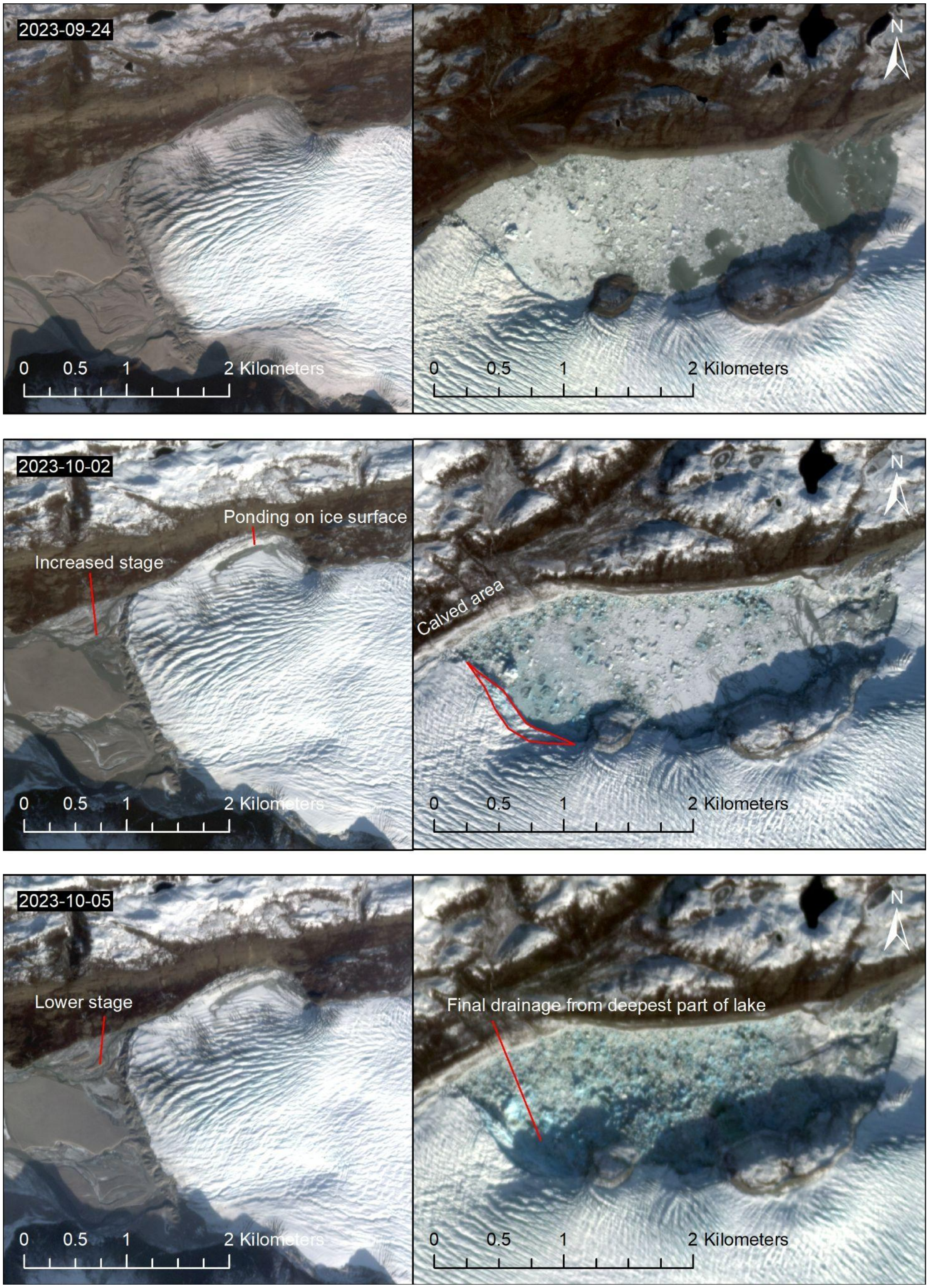

Figure 8. Cloud-free true colour optical satellite imagery (PlanetScope) of the terminus (left column) and ice-dammed lake (right column) before (24th September), during (2nd October) and after (5th October) the 2023 drainage event. Images © 2023 Planet Labs PBC.

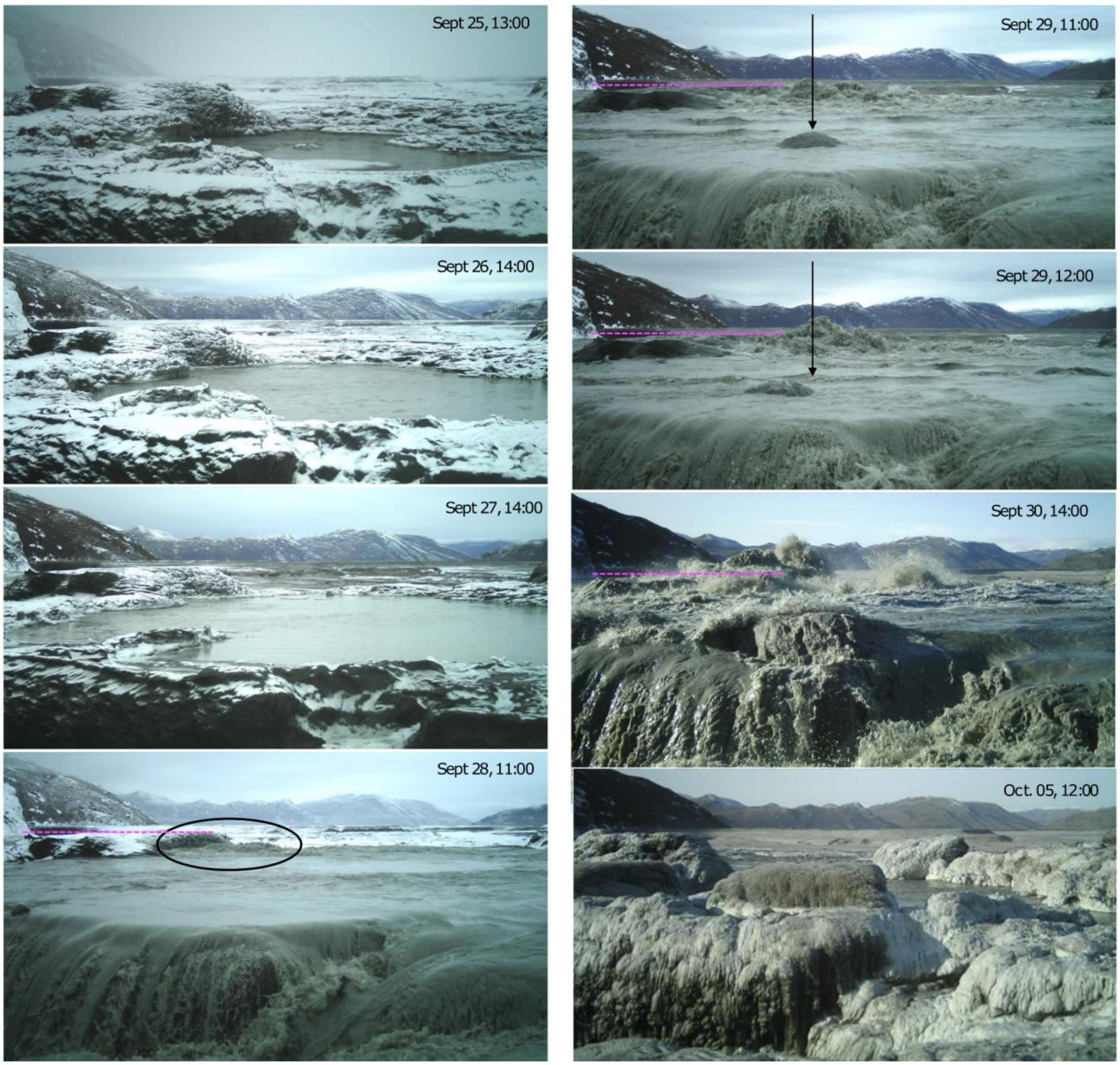

Figure 9. Time-lapse of the upwelling at the terminus of the glacier in 2023. Camera location: 67.181N -50.334W (Fig. 1 - Camera 4). Black circle highlights the point of turbulent upwelling. Pink dashed line is a water level reference line. Arrows on 29th September images highlight the formation and then movement of a mound of dislodged accreted ice or frozen outwash.

Passive seismic observations

During the first three weeks of September 2023, seismic energy in the frequency range 2-10 Hz gradually decreased at the foreland passive seismic station (Fig. 10a). This frequency range is characteristic of turbulent water flow (Gimbert and others, 2014), and the energy decrease was consistent with reduced runoff and proglacial river discharge in response to colder air temperatures during the late melt season. However, from 26th September, seismic energy began to increase rapidly, peaking around 2-4th October and then rapidly decreasing, with a pronounced period of low seismic energy on 5-6th October that fell below the longer term trend (Fig. 10b). The increase in seismic power was contemporaneous with an increase in river stage (Fig. 10b) suggesting that the record of seismic power can be used as a proxy for river discharge. During the subsequent melt event on 6-7th October, there was no correlation between high seismic energy and river stage (Fig. 10c), potentially reflecting a shift in where water is discharging from under the ice.

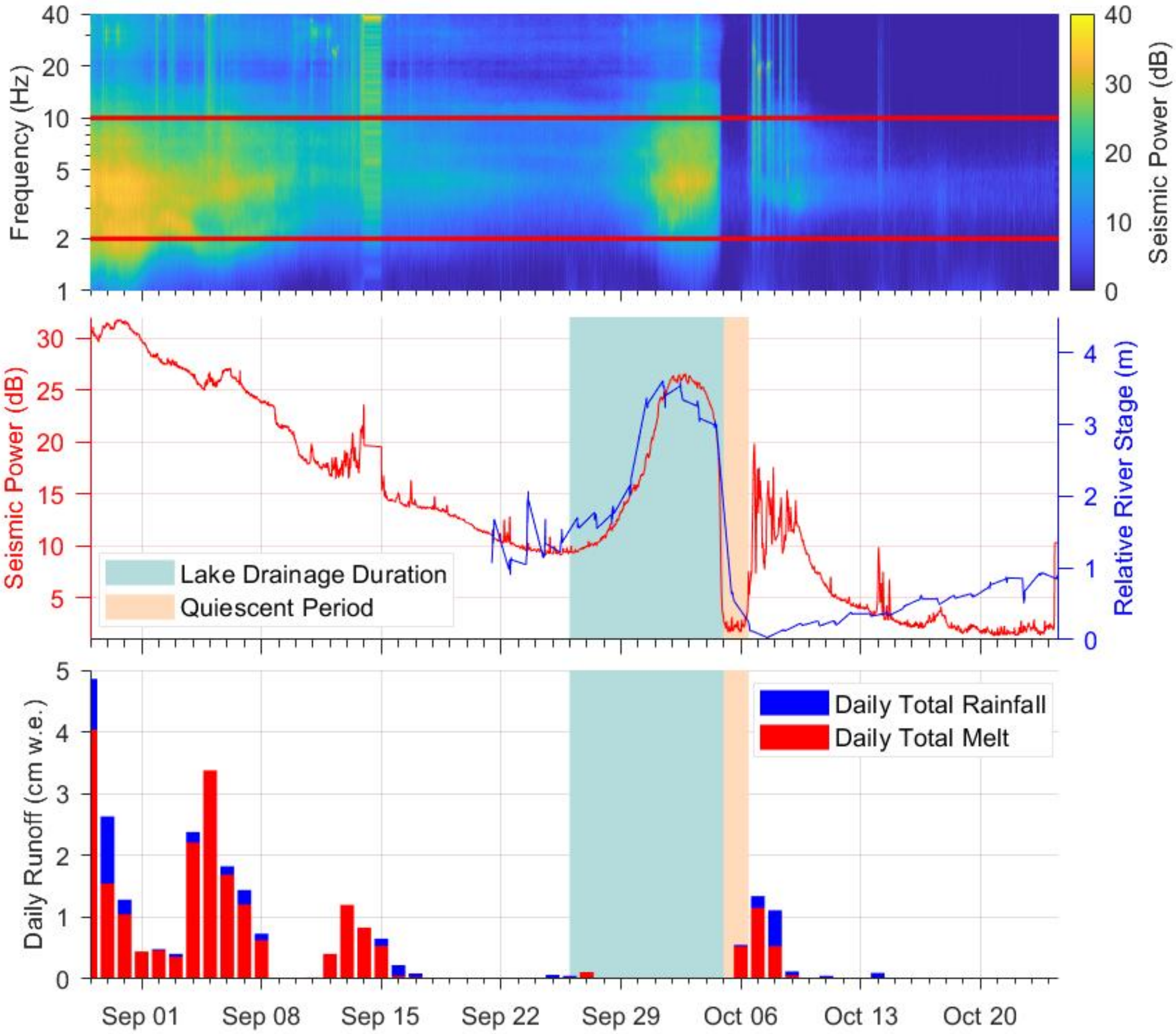

Fig. 10. (a) The passive seismic record from the forefield of Isunnguata Sermia from 29th August 2023 to 24th October 2023. Location of the terminus passive seismic station is marked in Figure

1. (b) Average seismic power within the 2-10 Hz frequency range (marked by the red lines in panel a). Note, the GLOF is picked out by a rapid increase in seismic energy (red line) starting on 26th September and peaking around 2-4th October (green shading), before rapidly decreasing. From 5-6th October there is a distinct low in seismic energy (orange shading). The change in seismic power is consistent with changes in relative proglacial river stage during the GLOF (blue line). (c). COSIPY daily total melt and rainfall at the GNSS site.

Ice dynamic observations

At the glacier scale, there was a 50-100 m yr^{-1} speed-up of ice flow into the southwestern ice-contact boundary of the ice-dammed lake and across the northern part of the terminus during the 2023 GLOF (Fig. 11, Fig. S5). The latter coincided with the emergence of turbid meltwater at the ice surface (Fig. 8). More generally, there was a slight ~20 m yr^{-1} speed-up of the tongue of Isunnguata Sermia downstream of the ice-dammed lake during the period when the lake drained (Fig. 11c). This acceleration was related to an increase in westerly flow, particularly over the central part of the tongue, and greater spreading of the near-terminus (Fig. S5). However, this magnitude of speed-up was similar to areas upstream of the lake, although they tended to have a patchier spatial signal.

The GNSS station, located 1-2 km up-glacier from the inferred drainage route of the ice-dammed lake (Fig. 7a), also recorded evidence of a change in ice dynamics during the 2023 GLOF (Fig. 12). There was a subtle increase in daily average horizontal velocity during the GLOF (from ~75 m yr^{-1} to ~80 m yr^{-1}) between 23rd September and 3rd October (Fig. 12a), although the initial speed up coincided with a small rainfall event on 24th September (Fig. 12c). This velocity increase was accompanied by a switch from ice-surface uplift to ice-surface subsidence of several centimetres over about 7 days (Fig. 12b). On 4-5th October horizontal velocity increased sharply, peaking at 93 m yr^{-1} on 5th October (Fig. 12a,d), and there was a steepening of the subsidence signal (~1 cm/day), which continued until 7th October (Fig. 12b,e). The velocity spike and increased subsidence lagged maximum lake discharge by 1-2 days and coincided with shutdown of the proglacial drainage system (Figs. 8-10). The trajectory of the GNSS also shifted slightly during the GLOF, temporarily trending further northwards towards the ice-dammed lake (Fig. 12d,e) until 7th October. A velocity spike of >100 m yr^{-1}, and a switch to ice-surface uplift, on 7-8th October was attributed to a melt and rainfall event (Fig. 12c).

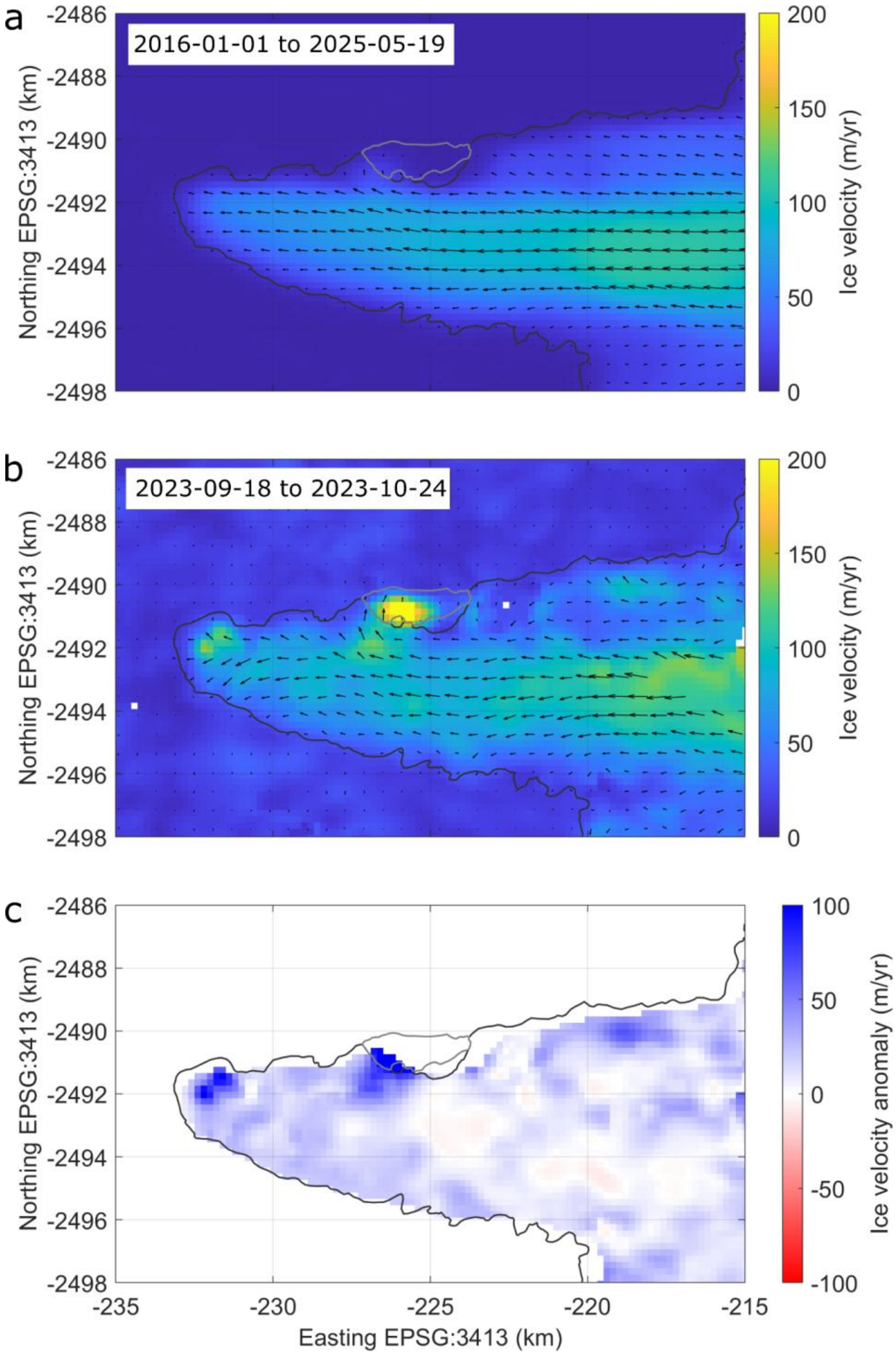

Fig. 11. Isunnguata Sermia ice velocity: a. 2016 - 2025 average ice velocity.; b. Average ice velocity for image pairs that include the 2023 ice-dammed lake drainage. Arrows in (b) and (c) are flow direction vectors and magnitudes; c. Ice velocity anomaly for the 2023 ice-dammed lake drainage period compared to the long-term average. Positive values (blue) represent pixels for which ice velocity was greater during the lake drainage period.

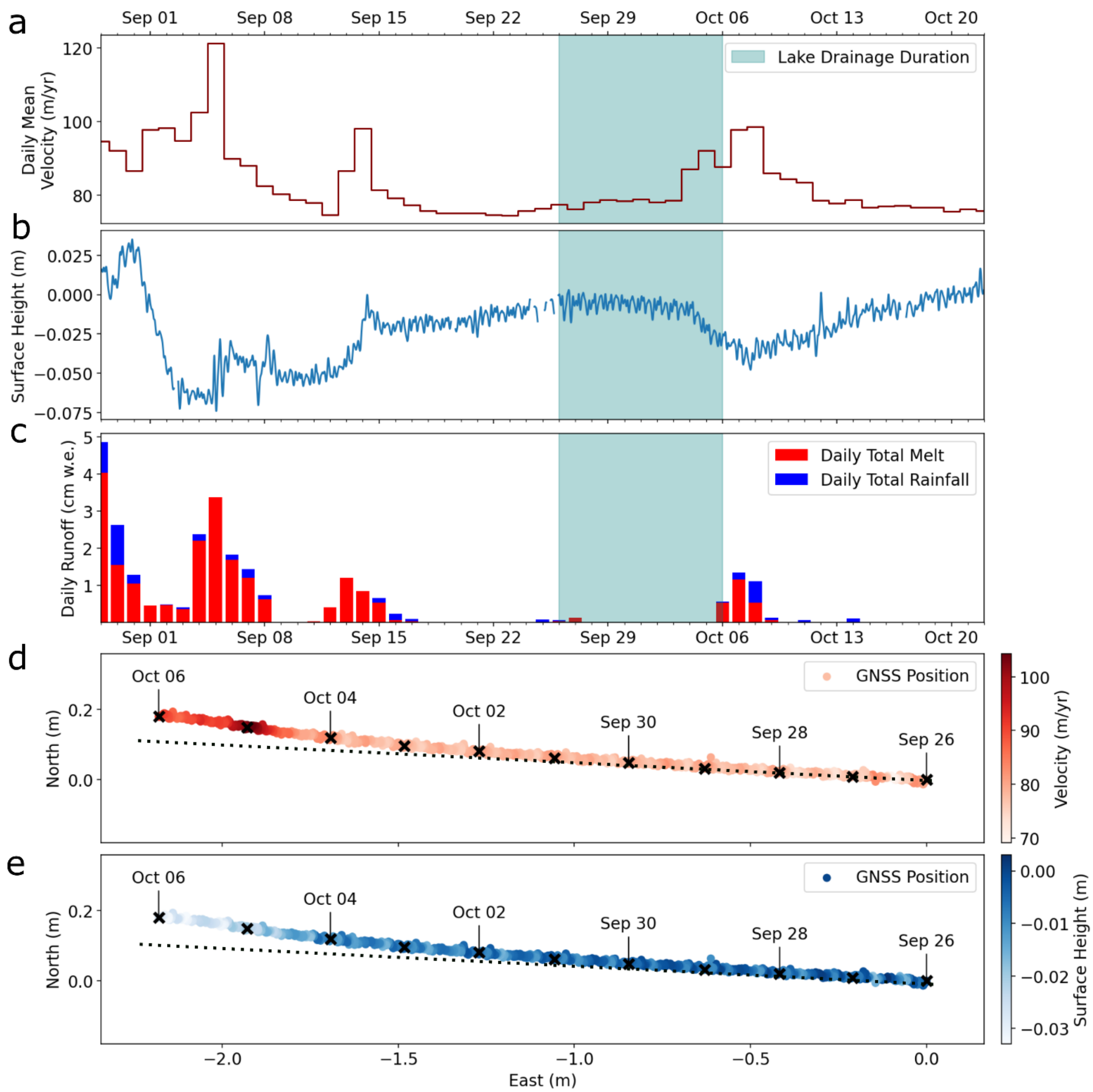

Fig. 12. Ice surface motion recorded by GNSS C in 2023: a. Daily mean horizontal surface velocity; b. Ice-surface elevation change; c. COSIPY daily total melt and rainfall at GNSS-C; d. The track of the GNSS coloured by 6-hr average horizontal velocity anomaly. e. As for (d) but coloured by elevation deviation relative to 26th September 00:00. The green shade highlights the period of lake drainage and corresponds to the time period of subplots (d) and (e). The dotted lines in (d) and (e) represent an extrapolation of the linear fit from 26-27th September

DISCUSSION

We have reconstructed the evolution of a large (0.218 ± 0.040 km^3) ice-dammed lake at the northern margin of Isunnguata Sermia, West Greenland from remote sensing and field measurements. Our results reveal multiple fill-drain cycles with gradual filling of the lake followed by rapid subglacial drainage over multiple days with a periodicity of 1-3 years. These GLOF events impact downstream and upstream ice dynamics, subglacial hydrology and runoff.

GLOF magnitude and frequency

Reconstruction of lake-level evolution since 1987 reveals no obvious change in the frequency or annual timing of GLOFs over the 37-year study period, but a ~0.05 km^3 reduction in maximum lake volume and a ~20 m decrease in the maximum lake level since 2010. The general reduction in lake volume since 2010 appears to coincide with glacier thinning, which could have reduced the water pressure in the lake needed to approach or exceed the overburden pressure of the ice dam (Thorarinsson, 1939; Tweed and Russell, 1999). However, this relationship breaks down in some years; for example, the lake reached a greater volume in 2022 (0.168 ± 0.009 km^3) than in 2019 (0.151 ± 0.019 km^3). This variation might reflect error in the mapping process or the temporal availability of satellite imagery - missing the maximum lake level. Alternatively, changes in geometry might not be the sole cause of the variations in water level, with drainage not always occurring when the ice dam reaches flotation (e.g., Björnsson, 1992; Huss and others, 2007; Veh and others, 2023).

The reduction in lake volume does not lead to a reduction in GLOF frequency (Fig. 3a). This is consistent with recent large-scale studies (see also Veh and others, 2023; Rick and others, 2023). In Figure 13 we explore potential runoff controls on GLOF frequency by summing modelled daily discharge from the main outlet of Isunnguata Sermia (Mankoff et al., 2020) over the recharge period between GLOFs. Although used as a proxy of runoff for lake recharge, we note that the catchment for the ice-dammed lake is likely much smaller than the main outlet. Overall, there is no clear relationship between catchment runoff and lake recharge volume. However, six of the eight recharge periods exhibited similar peak lake volumes (0.149-0.167 km^3) and total catchment runoff (9.2-11.6 km^3), suggesting a similar rate of filling (Fig. 13).

There are two clear outliers in the fill-drainage cycles. The first is the 2007 to 2010 recharge period, which had the lowest total catchment runoff but an anomalously large (0.208 km^3) lake recharge volume (Fig. 13). One possible explanation is that our crude proxy of using total runoff from the main Isunnguata Sermia catchment misses changes in area of the lake’s catchment, driven by changing ice thickness and water pressure (e.g., Chu et al., 2016).

The other outlier is the 2012 to 2015 recharge period, which coincided with approximately double the catchment runoff (23.46 km^3) (Fig. 13). This discrepancy can be explained by changes in the stability of the ice dam. The preceding 2012 lake drainage, which occurred relatively early in the melt season (May-June), was not followed by substantial lake filling until 2013 (Fig. 3), despite the record melt that year (Nghiem and others, 2012). This behaviour indicates that during this period the lake experienced a net loss of water, with the most obvious route for increased water loss via the subglacial channel(s) created during the 2012 GLOF. This is consistent with elevated runoff in 2012 (Nghiem and others, 2012) causing melt-enlargement to exceed creep closure of subglacial channels (Röthlisberger, 1972), with the early season GLOF enabling the channel(s) to remain open as surface melt increased thereafter. Further evidence that the ice dam can allow water to escape is provided by slight decreases in lake volume in winter, when outputs must have exceeded inputs. This behaviour is more evident when the lake is fuller and water pressure therefore higher prior to 2015 (Figs. 2-3a) (Gilbert, 1971; Matthews and Clague, 1993).

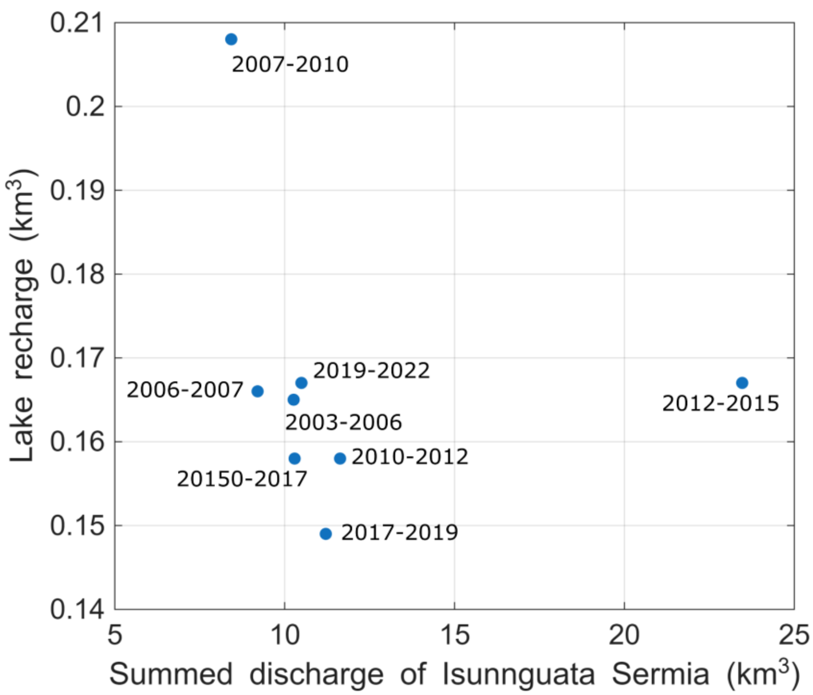

Figure 13. Summed discharge from the main outlet of Isunnguata Sermia (Mankoff and others, 2020) between drainage events of the ice-dammed lake against the change in lake volume over the same period where lake drainages are well constrained. The dates represent the period of lake filling (recharge).

Lake drainage mechanism: inferences from the 2023 GLOF

The rapid rising limb and sharp falling limb of the discharge hydrograph, inferred by the seismic and stage records at the terminus in 2023 (Fig. 10), is consistent with channelised drainage and the classical slow outburst flood model (Nye, 1976). However, at Isunnguata Sermia water emerges at multiple points along the terminus, suggesting a more complex multi-path drainage configuration. The spatial and temporal evolution of proglacial drainage and increase in downstream ice motion observed during the 2023 GLOF also suggests the channelised subglacial system was at least temporarily overwhelmed. Similar observations of other slow-rising GLOFs (Huss and others, 2007; Magnússon and others, 2007; Sugiyama and others, 2008) have been linked to water pressure exceeding ice overburden, driving water out of the channel, reducing basal friction and enabling other flowpaths to form (Clarke, 2003). Such short-term reconfiguration of subglacial systems highlights the importance of understanding the role of glacier lake drainage in local hydrologic and ice-dynamic perturbations.

Perturbation of the subglacial hydrological system

Subglacial water release during 2019 GLOF

The 2019 GLOF coincided with ice-surface subsidence in three downstream regions (Fig. 7a). Anomalies 1 and 3 are interpreted as distinct subglacial lakes based on their surface elevation time series of slow uplift (subglacial lake filling) followed by rapid subsidence (subglacial lake drainage) (e.g., Livingstone and others, 2019). The coincidence of the rapid drainage of these lakes with the 2019 ice-dammed GLOF suggests that GLOFs can trigger secondary releases of stored subglacial water along their flood path, which then contribute to output flood waters (e.g., Huss and others, 2007; Shangguan and others, 2017). Mejia and others (2021) suggest that subglacial flood waves from rapid supraglacial lake drainages can dewater isolated cavities by opening connections to them. Thus, we might expect release of stored water to be linked to GLOFs that have overwhelmed the subglacial drainage system causing vertical uplift and increased sliding, in turn leading to growth of cavities initiating new connections (Mejia and others, 2021). However, the 2019 GLOF occurred during peak melt season when we might expect the additional meltwater discharge from the GLOF to be largely accommodated by an efficient subglacial channelised system (Bartholomew and others, 2010); an interpretation supported by the absence of an observable ice-dynamic response (Fig. 5). An alternative mechanism is that the 2019 GLOF caused an increase in the local hydraulic gradient, possibly due to a pressure wave, or via expansion of low pressure channels, which was sufficient to trigger drainage of water stored subglacially (e.g., Jóhannesson, 2002; Kingslake and Ng, 2013; Dow and others, 2018). More generally, there is no obvious reason why the 2019 GLOF triggered the release of subglacially stored water compared to other years, suggesting a complex response that could also be related to the drainage route, antecedent conditions and stage of the subglacial lakes. This makes the estimation of proglacial discharges challenging.

The lack of a subsequent uplift pattern at Anomaly 2 following subsidence in 2019 suggests that either it was a subglacial lake that didn't refill once drained and therefore a transient feature, or given its position close to the meltwater outlet at the terminus, it could be recording collapse of ice above a subglacial channel (Egli and others, 2021; Hösli and others, 2025). The latter would be consistent with the GLOF causing rapid enlargement of the subglacial channel, thinning the ice roof and making it more prone to collapse. Although Anomaly 3 is even closer to the terminus, tunnel collapse might be favoured at Anomaly 2, for example, if it was over thinner ice or at a location where the hydraulic gradient is steeper resulting in greater turbulent melting of the subglacial channel roof.

Subglacial water storage after the 2023 GLOF

From 5-6th October, at the end of the 2023 GLOF, there is a distinct reduction in the observed seismic power to below the pre-event background signal, suggesting proglacial water flow is beneath the detectable threshold. This is supported by time-lapse imagery close to the glacier terminus, revealing an abrupt drop in water flow over the same period. This could reflect low melt inputs into the subglacial drainage system during this period, or a wider perturbation of the subglacial hydrology by the GLOF, temporarily inhibiting or changing the configuration of subsequent water flow from the wider catchment to the terminus. This contrasts with other studies that have observed a tail of above-average discharge thought to be associated with the release of stored water (e.g., Anderson and others, 2003; Huss and others, 2007). We postulate that the creation of large low-pressure channels (and potential evacuation of stored water similar to 2019) during the 2023 GLOF reduced the hydraulic gradient, initially inhibiting drainage (Dow and others, 2022) out of the overdeepened trough at Isunnguata Sermia (Lindbäck and others, 2014). Drainage up a reverse slope is supported by active ice accretion in the immediate foreland (Fig. 9), consistent with supercooled water (Cook and others, 2006; Cook and Swift, 2012). We suggest the relatively quiet seismic period from 5-6th October was characterised by re-pressurisation and re-filling of subglacial water stores until there was sufficient water to re-escape the overdeepening.

Ice dynamic response to GLOFs

At the western ice-water boundary of the ice-dammed lake, the latter stages of lake filling are typically characterised by ice-surface uplift (Fig. 4), indicating that water is penetrating up to ~200 m under the ice dam (either due to flexure or movement along fractures) causing flotation (e.g. Nye, 1976; Anderson and others, 2003; Walder and others, 2005; Bigelow and others, 2020). By neglecting subglacial storage, our lake volume estimates from satellite data therefore underestimate the volume of water. During GLOFs there is further evidence of mechanical damage, with calving of the marginal ice-front recorded by satellite data in multiple years (e.g., Figs. 6,8). This calving is likely driven by a rapid reduction in the hydrostatic pressure as the lake drains and the ice-front freeboard height increases.

The impact of ice-dammed lake drainage on ice velocity is variable (Fig. 5). Both the 2017 and 2019 GLOFs produced no detectable ice velocity signal in our Sentinel-1 data. These events occurred in August during peak melt season, and therefore we suggest the limited impact on ice motion is because the antecedent hydraulic capacity of the subglacial drainage system was sufficient to accommodate the additional water without spikes in water pressure (e.g., Livingstone and others, 2022). Indeed, there is also no observable change in the proglacial river and flood plain during the 2019 GLOF (Fig. 6) indicating that drainage was largely accommodated by the existing river system. In contrast, both the 2022 and 2023 GLOFs were associated with increased ice-flow downstream of the ice-dammed lake (Figs. 5, 11-12). Compared to 2019 the 2022 GLOF was of greater magnitude (mean discharge of 480 $m^3 s^{-1}$) and occurred earlier in the melt season (beginning of July) when the drainage system would have been more inefficient. It therefore follows that the 2022 GLOF was able to overwhelm the antecedent drainage system and elicit a detectable velocity response (e.g., Iken & Bindschadler, 1986; Kingslake and Ng, 2013).

The 2023 GLOF produced the largest observed downstream velocity anomaly (Fig. 5). This is consistent with the subglacial drainage system being overwhelmed due to its low antecedent hydraulic capacity after the end of the melt season (October), and following a period of declining melt and proglacial river flow. The larger acceleration of the northern part of the terminus (Fig. 11b-c) suggests the drainage system here was particularly sensitive to melt inputs. This is supported by the outflow of subglacial water to the ice surface through crevasses in this region (Fig. 8), suggesting high subglacial water pressures (Roberts, 2005; Roberts and others, 2010; Bowling and others, 2021). GNSS C, upstream of the ice-dammed lake, records an initial ~6% speed-up of ice flow and a switch from ice-surface uplift to subsidence between 24th September and 3rd October. This signal is consistent with longitudinal extension causing vertical compression of the ice at C, driven by downstream acceleration from increased basal sliding of the lower glacier tongue during the GLOF. The GNSS subsequently shows a sharp increase in ice-velocity and ice-surface subsidence from 4th October (Fig. 12), which lags peak discharge by ~1-2 days and is associated with ice flow deflection towards the ice-dammed lake. This is interpreted to record increased ice flow into the ice-dammed lake (Fig. 11b-c) as it re-adjusts following the rapid lowering of hydrostatic pressure (lake water-level drop) (Riesen and others, 2010), and re-grounding of floating ice causing an increase in driving stress.

CONCLUSIONS

We studied the evolution of a ~3 km^2 ice-dammed lake adjacent to the northern margin of Isunnguata Sermia, West Greenland that drains subglacially every 1-3 years. We used remote sensing observations to monitor lake volume changes between 1987 and 2024, and to quantify the downstream subglacial hydrological and ice dynamic impact. In 2023 a GLOF was instrumented with a number of sensors, including GNSS, a passive seismic station and time-lapse cameras deployed on and at the terminus of Isunnguata Sermia.

We demonstrate no clear change in the frequency or annual timing of GLOFs at Isunnguata Sermia, but a reduction in peak lake volume since 2010, likely due to glacier thinning in response to climate change. Predicting future changes in lake volume and drainage timing is complicated by the penetration of a wedge of water under the ice and leakage through the ice dam. In particular, net loss of water through the ice dam during the extreme melt year of 2012 suggests that some ice dams might become more leaky as the climate warms, reducing their potential to fill.

Our results demonstrate the potential for GLOFs to impact downstream ice dynamics and hydrology, and to trigger the release of water stored along the subglacial flood-path. The concomitant drainage of subglacial lakes during the 2019 GLOF demonstrates the potential for ice-dammed lake drainages to perturb the wider subglacial hydrological system. But the absence of similar releases of stored water during other GLOFs suggests antecedent subglacial hydrological conditions, drainage route and the impact of drainage on subglacial water pressure also impact this process.

Two ice velocity mechanisms were identified. The first velocity response, characterised by increased flow into the lake basin, is caused by the rapid removal of hydrostatic pressure at the lake-ice boundary and an increase in driving stress (ice-surface slope) following lake lowering. The second is increased basal sliding caused by the GLOF pressurising the subglacial drainage system. The impact of this is related to whether the discharge exceeds the hydrological capacity of the existing subglacial drainage system. In particular, GLOFs that occurred in the early- or late-melt season when subglacial drainage is inefficient elicited a greater ice velocity response.

Author contribution statement

The research was conceptualised by SL, RS and AS. SL wrote the manuscript with review and edits from RS, SD, RI, ST, AM, AS, TC, JG, CC, EB, KL, KW, BD, AHJ, SK, AB, AH and NR. Fieldwork to deploy and maintain the sensors was carried out by everyone other than AJ, AH and BD. BD automated the ice velocity processing and AS carried out the remote sensing of velocity. SD and AM processed the GNSS data. ST and FG processed the passive seismic data. ST also calculated river stage from the time-lapse imagery. SL

and RS carried out the shoreline mapping and reconstruction of freeboard height and water volumes. TC did the DEM production/ co-registration and RI the COSIPY modelling. Figures were produced by SL, RS, AM, AS, ST and KL. AJ produced the supplementary video of the upwelling. Funding for the project was acquired by SL, RS, SB, AS, KL, KW, JG, EB, NR, LE, BG, TH, MPJ and AB.

Acknowledgements

The SLIDE team was supported by NERC Grant NE/X000257/1. The NICE team was supported by NSF/NERC grants OPP-2039854 and NE/W004860/1, and is grateful for the support of Asiaq Greenland Survey. Both teams acknowledge the support of Kangerlussuaq International Science Support. TRC was supported by a Leverhulme Early Career Fellowship (ECF-2022-589). MPJ, JH and LC were supported by a UKRI Future Leaders Fellowship (MR/V022237/1). The ice-dammed lake shorelines, passive seismic data, time-lapse imagery and GNSS are available at the Polar Data Centre at XXXX. The authors thank the National Aeronautics and Space Administration [NASA]/USGS for the acquisition and free distribution of Landsat and ASTER images. The European Space Agency (ESA) is acknowledged for providing the Sentinel-1 data from the Copernicus Programme used in this study. We thank Planet Labs for providing access to their daily imagery through the education and research program. ArcticDEM is provided by the Polar Geospatial Center under NSF-OPP awards 1043681, 1559691, 1542736, 1810976, and 2129685. The PROMICE weather station data sets are available from How and others, (2022). Maps were created using QGIS.

References

Anderson SP and 6 others (2003) Integrated hydrologic and hydrochemical observations of Hidden Creek Lake jökulhlaups, Kennicott glacier, Alaska. J*ournal of Geophysical Research: Earth Surface*, 108(F1).

Bartholomew I, Nienow P, Mair D, Hubbard A, King MA, and Sole A (2010) Seasonal evolution of subglacial drainage and acceleration in a Greenland outlet glacier. *Nature Geoscience*, 3(6), pp.408-411.

Bigelow DG, Flowers GE, Schoof CG, Mingo LD, Young EM and Connal BG (2020) The role of englacial hydrology in the filling and drainage of an ice-dammed lake, Kaskawulsh Glacier, Yukon, Canada. *Journal of Geophysical Research: Earth Surface*, 125(2), p.e2019JF005110.

Björnsson H (1992) Jökulhlaups in Iceland: prediction, characteristics and simulation. *Annals of Glaciology*, 16, pp.95-106.

Bowling J and 10 others (2021) Surface outburst of a subglacial flood from the Greenland Ice Sheet. https://doi.org/10.21203/rs.3.rs-569793/v1.

Carrivick JL, Tweed FS (2013) Proglacial lakes: character, behaviour and geological importance. *Quaternary Science Reviews* 78 pp.34-52.

Carrivick JL and Quincey DJ (2014) Progressive increase in number and volume of ice-marginal lakes on the western margin of the Greenland Ice Sheet. *Global and Planetary Change*, 116, pp.156-163.

Carrivick JL and Tweed FS (2016) A global assessment of the societal impacts of glacier outburst floods. *Global and Planetary Change*, 144, pp.1-16.

Carrivick JL and Tweed FS (2019) A review of glacier outburst floods in Iceland and Greenland with a megafloods perspective. *Earth-Science Reviews*, 196, p.102876.

Carrivick JL and 9 others, (2022) Ice-marginal proglacial lakes across Greenland: Present status and a possible future. *Geophysical Research Letters*, 49(12), p.e2022GL099276.

Chen G (1998). GPS Kinematic Positioning for the Airborne Laser Altimetry at Long Valley, California (Massachusetts Institute of Technology).

Chu W, Creyts TT and Bell RE (2016) Rerouting of subglacial water flow between neighboring glaciers in West Greenland. *Journal of Geophysical Research: Earth Surface*, 121(5), pp.925-938.

Chudley TR and Howat IM (2024) pDEMtools: conveniently search, download, and process ArcticDEM and REMA products. *Journal of Open Source Software*, 9(102), p.7149.

Clarke GK (2003) Hydraulics of subglacial outburst floods: new insights from the Spring–Hutter formulation. *Journal of Glaciology,* 49(165), pp.299-313.

Cook SJ, Waller RI and Knight PG (2006) Glaciohydraulic supercooling: the process and its significance. *Progress in Physical Geography*, 30(5), pp.577-588.

Cook SJ and Swift DA (2012) Subglacial basins: Their origin and importance in glacial systems and landscapes. *Earth-Science Reviews*, 115(4), pp.332-372.

Davison BJ and 6 others, (2020) Subglacial drainage evolution modulates seasonal ice flow variability of three tidewater glaciers in southwest Greenland. *Journal of Geophysical Research: Earth Surface*, 125(9). doi:10.1029/2019jf005492

Díaz J, Ruíz M, Crescentini L, Amoruso A and Gallart J (2014). Seismic monitoring of an Alpine mountain river. *Journal of Geophysical Research: Solid Earth*, 119(4), pp.3276-3289.

Dømgaard M, Kjeldsen K, How P and Bjørk A (2024) Altimetry-based ice-marginal lake water level changes in Greenland. *Communications Earth & Environment*, 5(1), p.365.

Dow JM, Neilan RE and Rizos C (2009) The International GNSS Service in a changing landscape of Global Navigation Satellite Systems. *J. Geod.* 83, 191198.

Dow CF, and 6 others (2018) Dynamics of active subglacial lakes in Recovery Ice Stream. *Journal of Geophysical Research: Earth Surface*, 123(4), pp.837-850.

Einarsson B, Magnússon E, Roberts MJ, Pálsson F, Thorsteinsson T and Jóhannesson T (2016) A spectrum of jökulhlaup dynamics revealed by GPS measurements of glacier surface motion. *Annals of Glaciology*, 57(72), pp.47-61.

Einarsson B, Jóhannesson T, Thorsteinsson T, Gaidos E and Zwinger T (2017) Subglacial flood path development during a rapidly rising jökulhlaup from the western Skaftá cauldron, Vatnajökull, Iceland. *Journal of Glaciology*, 63(240), pp.670-682.

Evans SG and Clague JJ (1994) Recent climatic change and catastrophic geomorphic processes in mountain environments. In *Geomorphology and Natural Hazards* (pp. 107-128). Elsevier.

Flowers GE, Björnsson H, Pálsson F and Clarke GK (2004) A coupled sheet-conduit mechanism for jökulhlaup propagation. *Geophysical Research Letters*, 31(5).

Fowler AC and Ng FSL (1996) The role of sediment transport in the mechanics of jökulhlaups. *Annals of Glaciology*, 22, pp.255-259.

Gilbert R (1971) Observations on ice-dammed summit lake, British Columbia, Canada. *Journal of Glaciology*, 10(60), pp.351-356.

Gimbert F, Tsai VC and Lamb MP (2014) A physical model for seismic noise generation by turbulent flow in rivers. *Journal of Geophysical Research: Earth Surface*, 119(10), pp.2209-2238.

Glen JW (1954) The stability of ice-dammed lakes and other water-filled holes in glaciers. *Journal of Glaciology*, 2(15), pp.316-318.

Grinsted A, Hvidberg CS, Campos N and Dahl-Jensen D (2017). Periodic outburst floods from an ice-dammed lake in East Greenland. *Scientific Reports*, 7(1), p.9966.

Guizar-Sicairos M, Thurman ST, and Fienup JR (2008) Efficient subpixel image registration algorithms. *Optics Letters*, 33(2), 156. https://doi.org/10.1364/OL.33.000156

Haeberli W (1983) Frequency and characteristics of glacier floods in the Swiss Alps. *Annals of Glaciology*, 4, pp.85-90.

Hösli L and 10 others (2025) Subglacial cavity collapses on Swiss glaciers: spatio-temporal distribution and mass loss contribution. *Journal of Glaciology*, pp.1-35.

How, P and 10 others (2021). Greenland-wide inventory of ice marginal lakes using a multi-method approach. *Scientific reports*, 11(1), p.4481.

How P and others (2025) PROMICE and GC-Net automated weather station data in Greenland. doi:10.22008/FK2/IW73UU.

Iken A and Bindschadler RA (1986) Combined measurements of subglacial water pressure and surface velocity of Findelengletscher, Switzerland: conclusions about drainage system and sliding mechanism. *Journal of Glaciology*, 32(110), pp.101-119.

Jóhannesson T (2002) Propagation of a subglacial flood wave during the initiation of a jökulhlaup, *Hydrol. Sci. J.,* 47, 417–434.

Huss M, Bauder A, Werder M, Funk M and Hock R (2007) Glacier-dammed lake outburst events of Gornersee, Switzerland. *Journal of Glaciology*, 53(181), pp.189-200.

King O, Bhattacharya A, Bhambri R and Bolch T (2019) Glacial lakes exacerbate Himalayan glacier mass loss, *Sci. Rep.,* 9, 18145.

King M (2004). Rigorous GPS data-processing strategies for glaciological applications. *J. Glaciol.* 50, 601607.

Kingslake J and Ng F (2013) Modelling the coupling of flood discharge with glacier flow during jökulhlaups. *Annals of Glaciology*, 54(63), pp.25-31.

Kirillov A and 10 others (2023) Segment anything. In *Proceedings of the IEEE/CVF International Conference on Computer Vision* (pp. 4015-4026).

Kirkbride MP (1993) The temporal significance of transitions from melting to calving termini at glaciers in the central Southern Alps of New Zealand. *The Holocene*, 3(3), pp.232-240.

Kjeldsen KK, Khan SA, Bjørk AA, Nielsen K and Mouginot J (2017) Ice-dammed lake drainage in west Greenland: Drainage pattern and implications on ice flow and bedrock motion. *Geophysical Research Letters*, 44(14), pp.7320-7327.

Lea JM (2018) The Google Earth Engine Digitisation Tool (GEEDiT) and the Margin change Quantification Tool (MaQiT)–simple tools for the rapid mapping and quantification of changing Earth surface margins. *Earth Surface Dynamics*, 6(3), pp.551-561.

Liestøl O (1956) Glacier dammed lakes in Norway. *Norwegian Journal of Geography*,15:3-4, 122-149. https://doi.org/10.1080/00291955608542772

Lindbäck K and 8 others (2014) High-resolution ice thickness and bed topography of a land-terminating section of the Greenland Ice Sheet. *Earth System Science Data*, 6(2), pp.331-338.

Livingstone SJ, Sole AJ, Storrar RD, Harrison D, Ross N and Bowling J (2019). Brief communication: Subglacial lake drainage beneath Isunguata Sermia, West Greenland: geomorphic and ice dynamic effects. *The Cryosphere*, 13(10), pp.2789-2796.

Livingstone SJ and others (2022) Subglacial lakes and their changing role in a warming climate. *Nature Reviews Earth & Environment*, 3(2), pp.106-124.

Lützow N, Veh G and Korup O (2023) A global database of historic glacier lake outburst floods. *Earth System Science Data Discussions*, 2023, pp.1-27.

Magnússon E, Rott H, Björnsson H and Pálsson F (2007). The impact of jökulhlaups on basal sliding observed by SAR interferometry on Vatnajökull, Iceland. *Journal of Glaciology*, 53(181), pp.232-240.

Mallalieu J, Carrivick JL, Quincey DJ and Raby CL (2021) Ice-marginal lakes associated with enhanced recession of the Greenland Ice Sheet. *Global and Planetary Change,* 202, p.103503.

Mankoff KD and 9 others (2020) Greenland liquid water discharge from 1958 through 2019. *Earth System Science Data*, 12(4), pp.2811-2841.

Mathews WH and Clague JJ (1993) The record of jökulhlaups from Summit Lake, northwestern British Columbia. *Canadian Journal of Earth Sciences*, 30(3), pp.499-508.

Morlighem M and 10 others (2017) BedMachine v3: Complete bed topography and ocean bathymetry mapping of Greenland from multibeam echo sounding combined with mass conservation. *Geophysical Research Letters*, 44(21), pp.11-051.

Morlighem M, and others (2022) IceBridge BedMachine Greenland (IDBMG4, Version 5) [Data set]. Boulder, Colorado USA. *NASA National Snow and Ice Data Center Distributed Active Archive Center*. https://doi.org/10.5067/GMEVBWFLWA7X

Muñoz-Sabater J and others (2021) ERA5-Land: a state-of-the-art global reanalysis dataset for land applications. *Earth System Science Data* 13(9), 4349–4383. doi:10.5194/essd-13-4349-2021.

Ng F and Liu S (2009) Temporal dynamics of a jökulhlaup system. *Journal of Glaciology*, 55(192), pp.651-665.

Nghiem SV and 8 others (2012) The extreme melt across the Greenland ice sheet in 2012. *Geophysical Research Letters*, 39(20).

Nuth C and Kääb A (2011) Co-registration and bias corrections of satellite elevation data sets for quantifying glacier thickness change. *The Cryosphere*, 5(1), 271-290. https://doi.org/10.5194/tc-5-271-2011.

Nye JF (1976) Water flow in glaciers: jökulhlaups, tunnels and veins. *Journal of Glaciology*, 17(76), pp.181-207.

Post A and Mayo LR (1971) Glacier dammed lakes and outburst floods in Alaska (No. 455). *US Geological Survey*.

Rick B, McGrath D, McCoy SW and Armstrong WH (2023) Unchanged frequency and decreasing magnitude of outbursts from ice-dammed lakes in Alaska. *Nature Communications*, 14(1), p.6138.

Riesen P, Sugiyama S and Funk M (2010) The influence of the presence and drainage of an ice-marginal lake on the flow of Gornergletscher, Switzerland. *Journal of Glaciology*, 56(196), pp.278-286.

Roberts MJ (2005) Jökulhlaups: a reassessment of floodwater flow through glaciers. *Reviews of Geophysics*, 43(1).

Roberts MJ, Russell AJ, Tweed FS and Knudsen Ó (2000) Ice fracturing during jökulhlaups: implications for englacial floodwater routing and outlet development. *Earth Surface Processes and Landforms*, 25(13), 1429-1446.

Röthlisberger H (1972) Water pressure in intra-and subglacial channels. *Journal of Glaciology*, 11(62), pp.177-203.

Russell AJ, Roberts MJ, Fay H, Marren PM, Cassidy NJ, Tweed FS and Harris T (2006) Icelandic jökulhlaup impacts: implications for ice-sheet hydrology, sediment transfer and geomorphology. *Geomorphology*, 75(1-2), pp.33-64.

Russell AJ, Carrivick JL, Ingeman-Nielsen T, Yde JC and Williams M (2011) A new cycle of jökulhlaups at Russell Glacier, Kangerlussuaq, West Greenland. *Journal of Glaciology*, 57(202), pp.238-246.

Sandwell D, Mellors R, Tong X, Wei M and Wessel P (2011a) An InSAR processing system based on Generic Mapping Tools. UC San Diego: Scripps Institution of Oceanography.

Sandwell D, Mellors R, Tong X, Wei M and Wessel P (2011b) Open radar interferometry software for mapping surface deformation. *Eos, Transactions American Geophysical Union*, 92(28), 234. https://doi.org/10.1029/2011EO280002

Sauter T, Arndt A and Schneider C (2020) COSIPY v1.3 – an open-source coupled snowpack and ice surface energy and mass balance model. *Geoscientific Model Development* 13(11), 5645–5662. doi:10.5194/gmd-13-5645-2020.

Schmandt B, Aster RC, Scherler D, Tsai VC and Karlstrom K (2013) Multiple fluvial processes detected by riverside seismic and infrasound monitoring of a controlled flood in the Grand Canyon. *Geophysical Research Letters*, 40(18), pp.4858-4863.

Shangguan D, Ding Y, Liu S, Xie Z, Pieczonka T, Xu J and Moldobekov B (2017). Quick release of internal water storage in a glacier leads to underestimation of the hazard potential of glacial lake outburst floods from Lake Merzbacher in Central Tian Shan Mountains. *Geophysical Research Letters*, 44(19), pp.9786-9795.

Sugiyama S, Bauder A, Huss M, Riesen P and Funk M (2008) Triggering and drainage mechanisms of the 2004 glacier-dammed lake outburst in Gornergletscher, Switzerland. *Journal of Geophysical Research: Earth Surface*, 113(F4).

Sutherland JL, Carrivick JL, Gandy N, Shulmeister J, Quincey DJ and Cornford S (2020) Proglacial lakes control glacier geometry and behavior during recession. *Geophysical Research Letters*, 47(19), p.e2020GL088865.

Thorarinsson S (1939) Chapter IX. The ice dammed lakes of Iceland with particular reference to their values as indicators of glacier oscillations. *Geografiska Annaler,* 21(3–4), 216–242. https://doi.org/10.1080/20014422.1939.11880679.

Tomczyk, AM, Ewertowski MW and Carrivick JL (2020) Geomorphological impacts of a glacier lake outburst flood in the high arctic Zackenberg River, NE Greenland. *Journal of Hydrology*, 591, p.125300.

Tweed FS and Russell AJ (1999) Controls on the formation and sudden drainage of glacier-impounded lakes: implications for jökulhlaup characteristics. *Progress in Physical Geography*, 23(1), pp.79-110.

Tuckett PA and 6 others (2019) Rapid accelerations of Antarctic Peninsula outlet glaciers driven by surface melt. *Nature Communications*, 10. doi:10.1038/s41467-019-12039-2

Veh G and 8 others (2023) Less extreme and earlier outbursts of ice-dammed lakes since 1900. *Nature*, 614(7949), pp.701-707.

Walder JS and 6 others (2005) Fault-dominated deformation in an ice dam during annual filling and drainage of a marginal lake. *Annals of Glaciology*, 40, pp.174-178.

Welch PD (1967) The use of fast Fourier transform for the estimation of power spectra: A method based on time averaging over short, modified periodograms. *IEEE Transactions on Audio and Electroacoustics* 15(2): 70–73.

Whalley WB (1971) Observations of the drainage of an ice-dammed lake – Strupvatnet, Troms, Norway. *Norsk Geografisk Tidsskrift* 25, 165–74.

SUPPLEMENTARY FIGURES

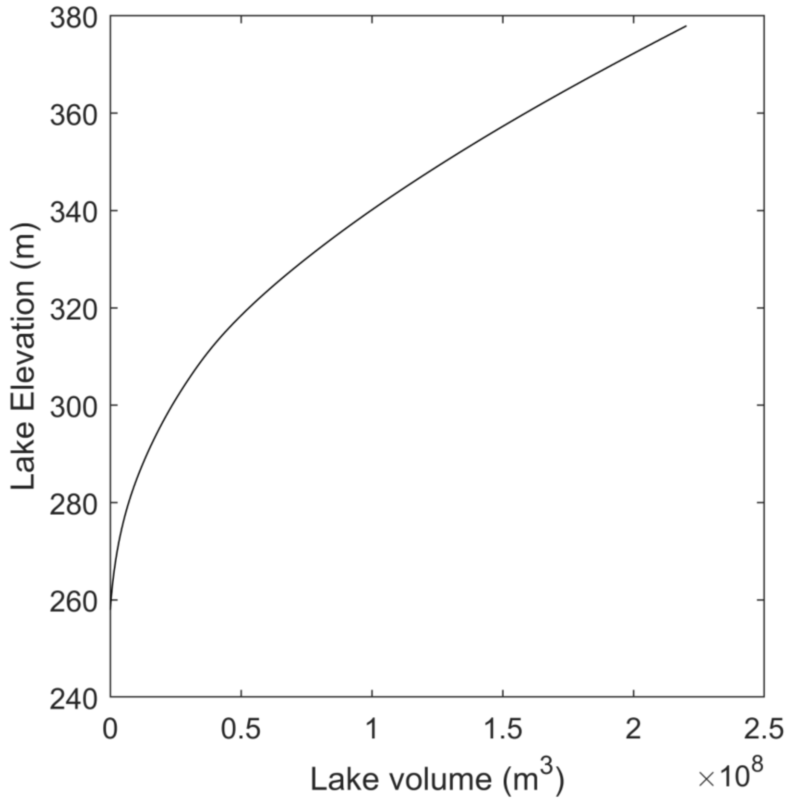

Figure S1. Elevation-Volume scaling relationship derived from the 11/08/2019 ArcticDEM DSM strip when the lake was empty.

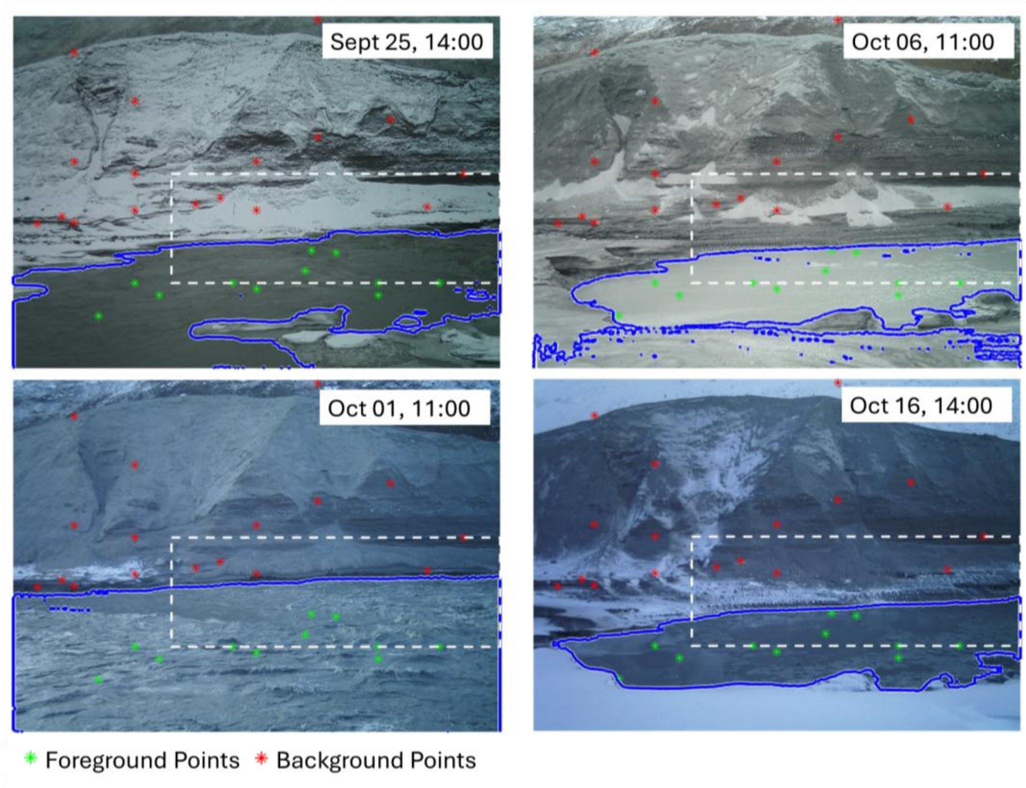

Figure S2. Examples of the Time-lapse imagery used to estimate the river stage at the terminus of the glacier in 2023. Camera location: -50.334W 67.181N -50.335W (Fig. 1 - Camera 3). Red and green stars show the background and foreground points used in the Segment Anything Model (SAM). Blue line is the output of the SAM showing the water mask. The height of the water mask averaged in the area delineated by the white dotted line is taken as the relative river stage.

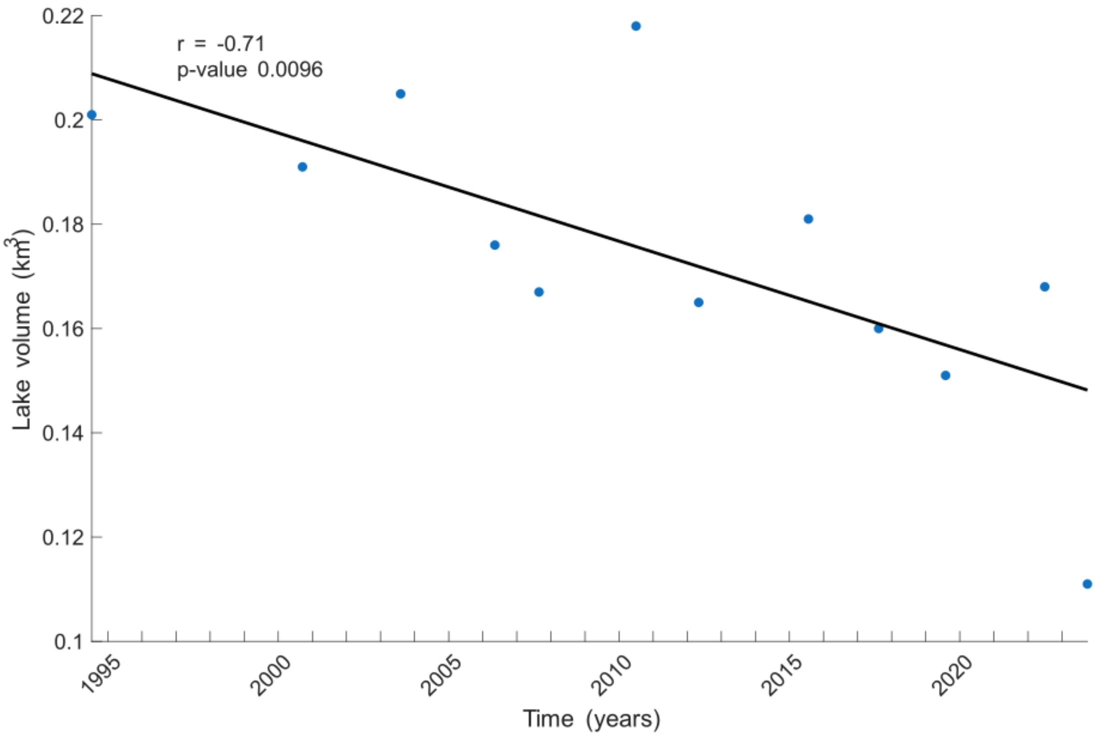

Figure S3. Robust linear regression of maximum pre-drainage lake volume through time. A statistically significant negative linear relationship was observed (Pearson r = -0.71, p = <0.05).

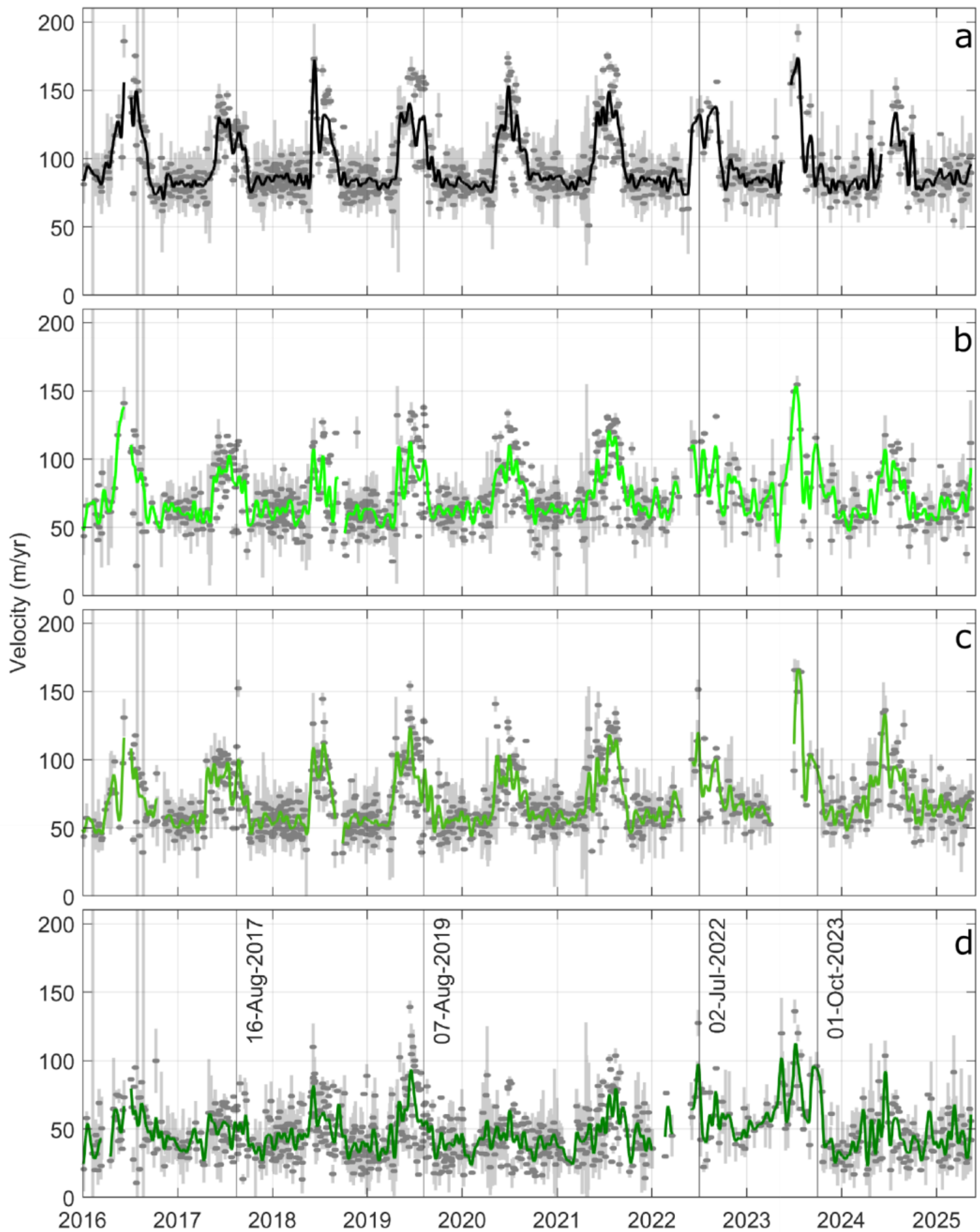

1034

1035 **Figure S4.** Ice velocity time-series for ROIs D1-3 and U1 (see Fig. 1 for locations). (a) is the U1
1036 time-series, and (b-d) are the D1 to D3 times-series, respectively.

1037

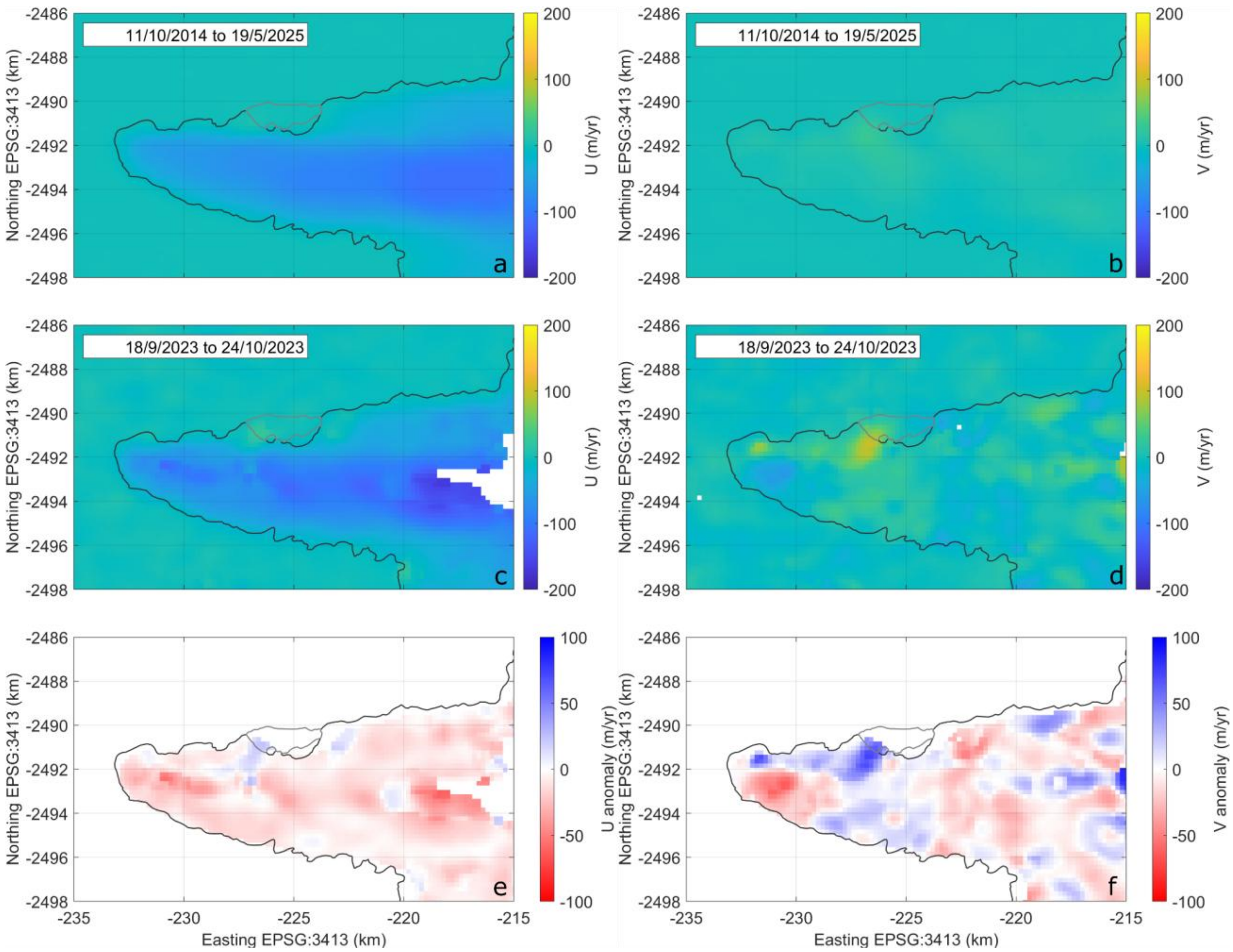

Figure S5. Isunnguata Sermia ice velocity: a-b. 2014 - 2025 average ice velocity of the U and V components, respectively; c-d. Average ice velocity of the U and V components for image pairs that include the 2023 ice-dammed lake drainage; e-f. Ice velocity anomaly in the U and V direction for the 2023 ice-dammed lake drainage period compared to the long-term average. Positive values (blue) represent pixels for which ice velocity was greater during the lake drainage period.